OLIGOFLUORENE ANTENNAE FOR LUMINESCENT LANTHANIDE CATIONS: SYNTHESIS AND CHARACTERIZATION

by

David Samuel Oxley

B.S., Virginia Polytechnic Institute and State University, 2004

Submitted to the Graduate Faculty of

Arts and Sciences in partial fulfillment

of the requirements for the degree of

Master in Sciences

University of Pittsburgh

2007

UNIVERSITY OF PITTSBURGH

ARTS AND SCIENCES

This thesis was presented

by

David Samuel Oxley

It was defended on

February 22, 2007

and approved by

Alexander Star, Assistant Professor, Department of Chemistry

Tara Y. Meyer, Associate Professor, Department of Chemistry

Thesis Director: Stéphane Petoud, Assistant Professor, Department of Chemistry

**OLIGOFLUORENE ANTENNAE FOR LUMINESCENT LANTHANIDE CATIONS:
SYNTHESIS AND CHARACTERIZATION**

David Samuel Oxley, M.S.

University of Pittsburgh, 2007

Lanthanide complexes emit as sharp emission bands, have long luminescence lifetimes for

temporal discrimination from background fluorescence and strong resistance to photobleaching.

These attractive properties make lanthanide compounds potentially applicable in a variety of

devices, including optical displays and sensors. However, luminescent lanthanide cations weakly

absorb light, and require proximal chromophores to absorb excitation light. Energy is

subsequently transferred to the lanthanide cations, resulting in the sensitization of their emission.

Usually, the energy levels in a given chromophore are fixed and cannot be adjusted. In this

thesis, oligofluorene ligands, comprised of either one (*mono*) or three (*ter*) fluorene units in the

backbone, exhibited a tunable nature of their electronic levels directly controlled by the number

of fluorene units. By varying the length of the fluorene backbone in these ligands, the donating

level(s) of the chromophore was (were) discretely tuned to the accepting level(s) of a particular

lanthanide (Eu and Tb). Furthermore, the lanthanide cation was coordinated to a cage-like

polyaminocarboxylate moiety within the ligand, which protected the cation from non-radiative

deactivation. Matching the energies of the donating electronic states of an oligofluorene ligand

with the appropriate accepting levels of a lanthanide cation lead to efficient oligofluorene to

lanthanide energy transfer with quantum yields of 7%, such as in the $TF1:Eu^{3+}$ complex. The

efficiency in these novel lanthanide complexes is comparable to established lanthanide

compounds used today in fluoroimmunoassays.

TABLE OF CONTENTS

LIST OF TABLES

LIST OF FIGURES

1.0   INTRODUCTION

The goal of this project was to develop new antennae for luminescent lanthanide cations emitting in the visible region. These oligofluorene antennae have electronic structures which were modulated based on the size of the antennae. The construction of the luminescent lanthanide complexes was achieved by connecting a coordinating unit, diethylenetriaminepentaacetic acid (DTPA) to a backbone of fluorene units. This DTPA moiety coordinated the luminescent lanthanide cation. The discrete sizes of the fluorene moieties generated electronic structures which fine tuned the photophysical properties of the resulting luminescent lanthanide complexes.

2.0   LANTHANIDES

2.1   GENERAL PROPERTIES OF THE LANTHANIDES

The lanthanides are the elements from cerium to lutetium along the first row of the *f*-block on the

periodic table. These elements generally adopt the 3+ oxidation state, although the 2+ and 4+

states exist for some lanthanides[1]. The internal 4*f* orbitals (**Figure 1**) are shielded by the valence

5*s* and 5*p* orbitals. This shielding effect leads to photophysical properties unique to the

lanthanides. The lanthanides experience moderate crystal field splitting due to little interaction

Figure 1. Energy level diagrams for lanthanides displaying the energy levels of the f-orbitals.

2

with the surrounding environment. Thus, the emission bands of the lanthanides appear as sharp (atom-like) bands at fixed wavelengths (**Figure 2**).The emission bands of the lanthanides are narrower than those of organic molecules [2], and are present in both the visible and in the near-infrared (NIR) regions.
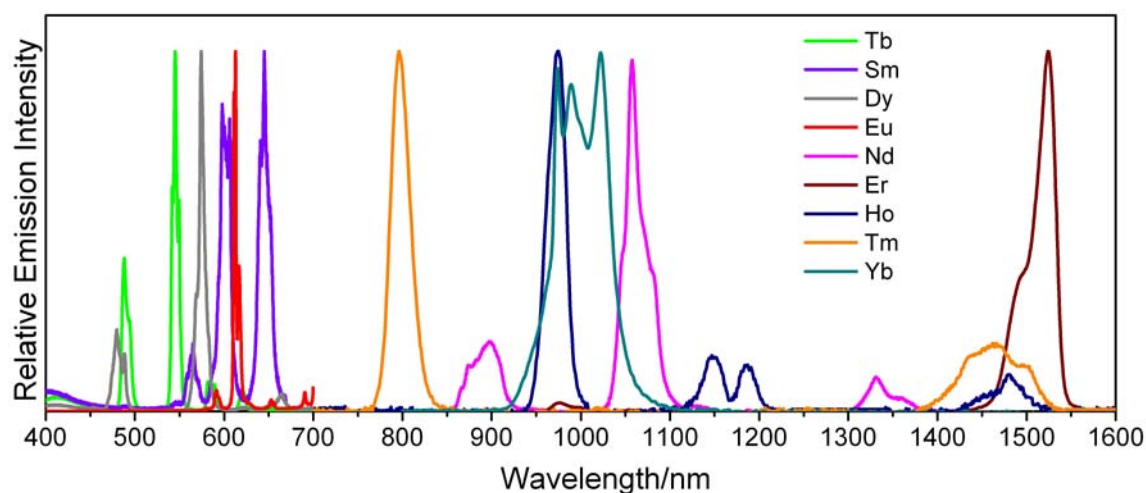
Figure 2. The sharp lanthanide emission bands in the visible and NIR regions. [3], [4]

2.2   ANTENNAE EFFECT

Since f-f transitions are forbidden by the Laporte rule, this results in low (on the order of <10 $M^{-1}cm^{-1}$) molar absorption coefficients for the lanthanide ions[5]. The forbidden transitions also induce long luminescence lifetimes (from a few microseconds to several milliseconds). Time-resolution of lanthanide compounds is possible, due to long lifetimes of the lanthanides, and facile discrimination from organic fluorescence and the background (autofluorescence) is common, and is yet another attractive property of lanthanides. The challenge to sensitize lanthanide emission, as Weissman reported[6], is to overcome the poor absorption ability, in order to take advantage of their unique photophysical properties. This is has been achieved by

coordinating lanthanide cations to organic chromophores. The process of the chromophores absorbing excitation light and transferring the resulting energy to the lanthanide cations is called the "antenna effect"[6] (**Figure 3**). The light is absorbed by the organic chromophore, the "antenna", to an excited singlet state. This undergoes intersystem crossing and subsequent population of the chromophore's triplet state occurs.
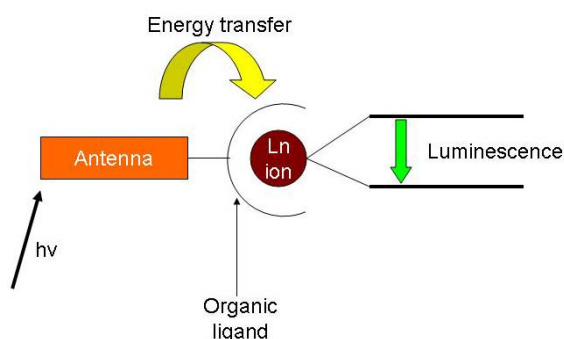
Figure 3. Schematic depiction of the antenna effect.

Energy transfer between the antennae and lanthanide cation occurs between the triplet state of the chromophore and the excited state of the lanthanide (**Figure 4**). There are competing processes which can influence the efficiency of the ligand to lanthanide energy transfer. Non-radiative relaxation, either of fluorescence from the excited singlet state or of phosphorescence from the excited triplet state, is common in organic chromophores. The chromophore and lanthanide are especially susceptible to deactivation if the energy levels of the triplet state of the chromophore and excited state of the lanthanide are not compatible. Overtone quenching (**Figure 5**) also plays a large role in non-radiative deactivation of excited states. Protection of the lanthanide cations by fulfilling their high coordination requirement is an efficient strategy to minimize non-radiative quenching.
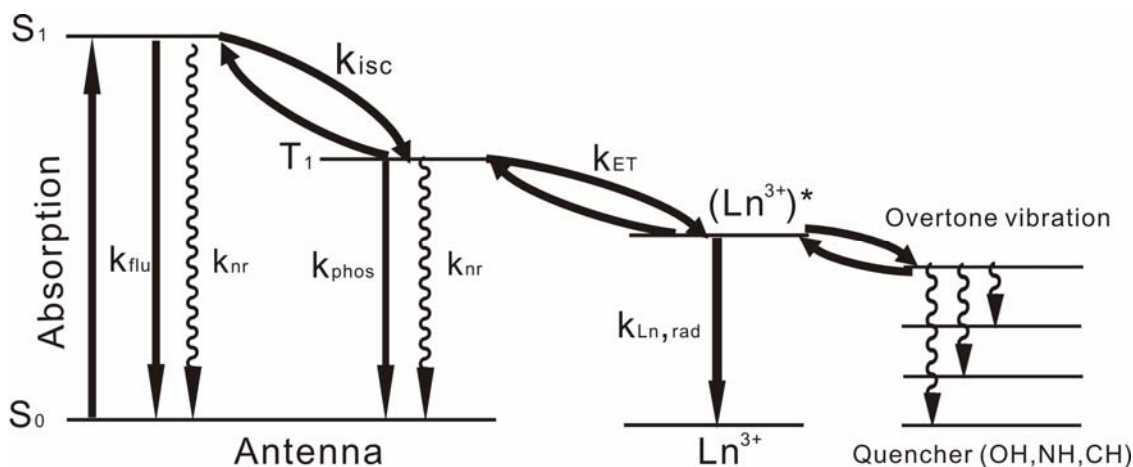
Figure 4. Jablonski diagram of lanthanide complex system (k_{flu} = rate of fluorescence decay; k_{nr} = rate of non-radiative decay; k_{isc} = rate of intersystem crossing; k_{phos} = rate of phosphorescence decay; k_{ET} = rate of energy transfer; $k_{Ln,rad}$ = rate of lanthanide radiative decay; S_0 = singlet ground state, S_1 = singlet excited state, T_1 = triplet state)

Two principal mechanisms govern energy transfer between the excited triplet state of the ligand and the excited states of the lanthanide. The Dexter mechanism is explained by electron-exchange[7]. In this theory, the donor (ligand) and acceptor (lanthanide) must physically exchange an electron. This exchange must be accompanied by direct contact between the orbitals of the donor and acceptor. The second mechanism is called the Förster mechanism[8], and is based on dipole-dipole interaction between the donor and acceptor. In this regime, the emission spectrum of the donor overlaps with the absorption spectrum of the acceptor as the energy traverses through space. The Förster mechanism is dependent on r^{-6}, where r is the distance between the donor and acceptor. A third mechanism exists, called electron transfer[9], but only arises if the overlap of donor's emission spectrum and the acceptor's absorption spectrum is poor. This sometimes occurs in compounds containing Eu^{3+} and Yb^{3+}.
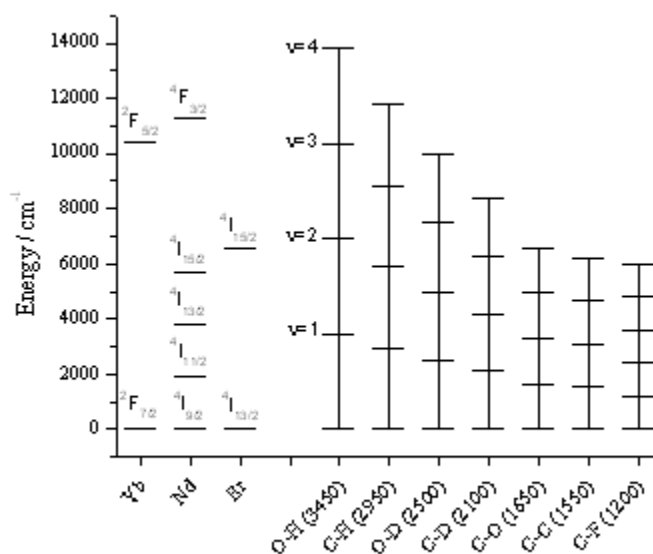
Figure 5. Vibrational overtones and their potential interactions with excited states of some NIR emitting lanthanides.

2.3   LANTHANIDE COMPLEXES

For lanthanide coordination, the ligand design is critical. To obtain good luminescence properties, good strategies include the complete protection of the lanthanide cation from sources of non-radiative deactivation and positioning the lanthanide in an area where energy can be transferred from chromophores. This chromophore must also efficiently harvest and light and subsequently transfer its energy to the lanthanide excited states, so the ligand must possess the appropriate structure to achieve this function. Lanthanide cations are hard Lewis acids. To form a strong hard-hard Lewis type of interaction, a ligand containing a hard base, such as a negatively-charged oxygen or nitrogen containing functional group, would be ideal. In addition, trivalent lanthanide cations in solution require coordination numbers of 8 to 12 for adequate protection from solvent molecules that could act as quenchers. Thus, a polydentate ligand with multiple hard base atoms would be an excellent choice for the coordination of lanthanides.

Diethylenetriaminepentaacetic acid (DTPA) and 1,4,7,10-tetraazacyclododecane- *N-N'-N''-N'''*-tetraacetic acid (DOTA) are common polyaminocarboxylate ligands (**Figure 6**), which combine the desired hard base characteristics with the polydentate scaffold[10]. Both ligands have multiple pendant arms which can be further functionalized with chromophores or alkyl spacer groups. Another ligand, triethylenetetraamine-hexaacetic acid (TTHA), has an additional polyaminocarboxylate group which has additional pendant arms available for the coordination and protection of the cation. However, Li and Selvin[11] report that the extra arms may interfere with the ability of the chromophore to donate energy efficiently.

DTPA   **DOTA**

TTHA
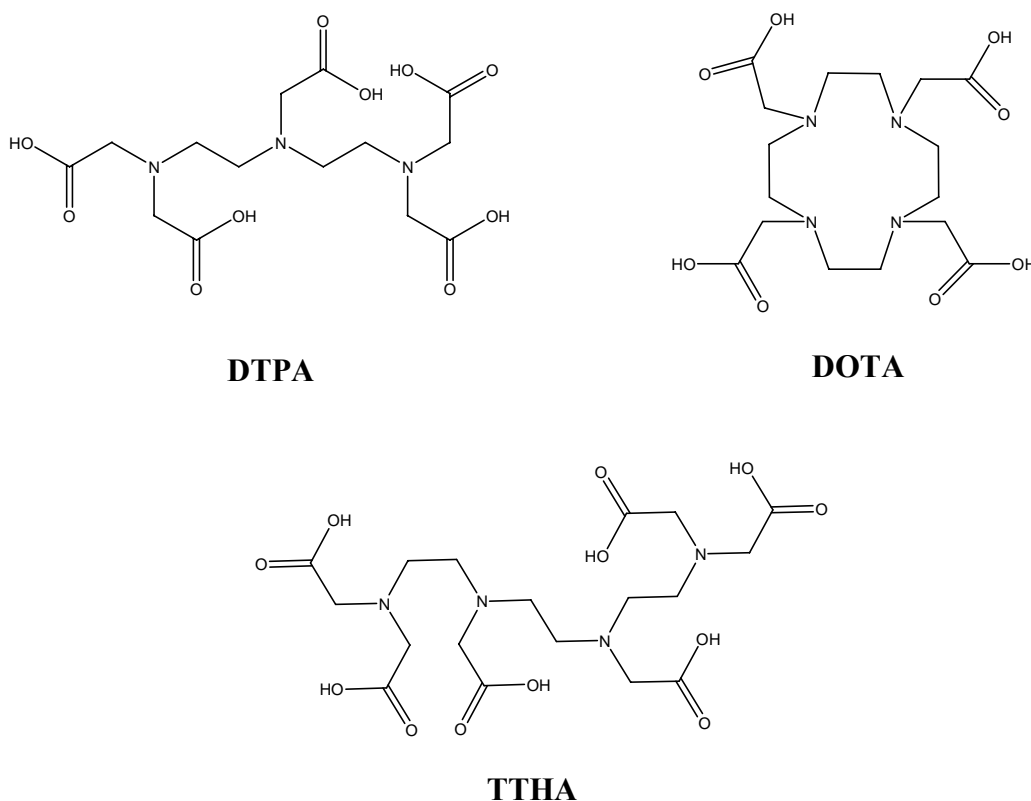
Figure 6. Common polyaminocarboxylate ligands.

3.0 OLIGOFLUORENE MOLECULES

3.1 STRUCTURE OF FLUORENE

Fluorene (**Figure 7**) is a small organic molecule comprised of a central five-membered ring attached to two adjacent aromatic six-membered rings. Fluorene is a rigid, planar unit, which influences its electronic properties. The planarity generates conjugation, leading to attractive photophysical properties. As fluorene units are connected along a backbone (**Figure 8**), the conjugation is further extended through delocalization. The electronic properties of the fluorene are influenced by the level of conjugation. This is commonly controlled by creating oligomeric segments of fluorene[12].
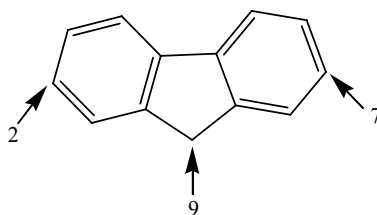
Figure 7. Fluorene with its 2, 7 and 9 positions highlighted.

A second attractive property of fluorene is its chemical functionality. The 2, 7 and 9 positions of fluorene are suitable sites for modification of the backbone. The 2 and 7 sites are typically reserved for connection to subsequent fluorene units or capping moieties. The two functional sites at the 9 position; however, are where the fluorene allows for versatile, chemical functionalization. This position can be alkylated to increase solubility[13], or to provide adequate

spacing between adjacent backbones. Side chains located at this position have also been attached

to control the performance of the fluorescence emitter in light-emitting diode (LED) devices[14].

Furthermore, functionalizing the 9 position does not greatly alter the electronic properties of the

conjugated fluorene backbone[15].
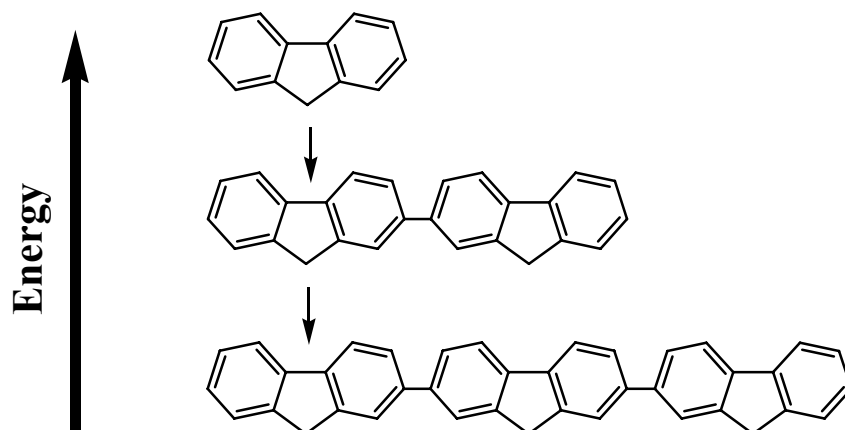
Figure 8. As conjugation in a fluorene backbone increases by attaching additional units, the overall energy of the orbitals, through delocalization, decreases.

3.2   ELECTRONIC PROPERTIES OF FLUORENE

The intensely blue-emitting fluorene is produced by its conjugated network. Polyfluorene has a

broad absorption band at ~350 nm due to the highly absorptive π-π* transition[16]. The broad

absorption is credited to the distribution of chain lengths in the polymer. Emission of

polyfluorene appears as three bands centered around 400 nm. Respectively, these are the 0→0,

0→1 and 0→2 intrachain transitions, with the first band typically being the most intense.

Photoluminescence quantum yields of fluorene species are usually large, with reported values in

solution and solid state over 70%[17]. The energy position of the π-π* transition depends on the

conjugation length. Fluorene possesses a special ability to create well-defined oligomers.

Fluorene's effective conjugative length, the minimum number of aromatic rings necessary for

saturation of electronic and optical properties, is 24 (12 fluorene units)[12]. Therefore, by creating oligofluorenes with less than 12 units the absorption can be tuned to discrete, well-defined energies.

Planarity and controlled spacing between planes helps maintain an optimal distance between fluorene chains, preserving fluorescence efficiency and minimizing degradation. Firstly, the preservation of planarity affects the effective conjugation length and absorption energy of the fluorene[18]. If buckling or torsion along the backbone occurs, effective conjugation length decreases. This is because adjacent segments along the chain are no longer in the same plane and the p orbitals are forced out of the same electron cloud. Steric interference of substituents along the backbone may also compromise planarity[19]. Spacing between adjacent planes is aided by alkylating the 9 position to keep the planes at a fixed distance, minimizing π-stacking and interchain energy transfer. Liu et al.[15] probed the fluorene emission as a function of side chain length by examining fluorescence lifetimes and quantum yields. Their studies measured the effects of the side chain length on fluorescence resonance energy transfer (FRET)[15]. Efficiency of FRET is increased for the shorter chains if solvent interactions were accounted for. A crucial property must be upheld: choosing a chain length that works within an FRET-acceptable distance and keeps adjacent chains at the sufficient distance to minimize interchain interactions and aggregation[20].

Photoinduced degradation[21] is a main deterrent in keeping a defect-free fluorene chain. Chemical oxidation of the fluorene produces a carbonyl group at the 9 position (also called an aromatic ketone or fluorenone), which is an active fluorescence quencher. Cheon et al.[22] report that attaching bulky substituents, such as their 4-dicyanomethylene-2-methyl-6-(bis(4'-bromophenyl)amino)styryl-4*H*-pyran (DCM), suppresses defects along the polymer chain and

reduces the undesired long wavelength emission. Indeed, substitution at the 9 position should diminish its susceptibility to oxidation. Another approach to minimize photodegradation capitalizes on the fast and efficient energy transfer within conjugated polymers[23]. Utilizing fluorene as a donor will channel the energy away and provide efficient transfer to an acceptor which serves as a fluorescent emitter.

3.3   FLUORENE AS AN ENERGY DONOR

There has been much effort to use fluorene as an energy donor because of its robust photo-physical properties. Its fast energy transfer within segments in the chain shifts emission to longer wavelengths[22]. The processes of decay through the lowest vibrational level of the singlet state, S_1, intersystem crossing and subsequent vibrational relaxation to the lowest energy triplet state, T_1, is about 1 nanosecond for most conjugated polymers[24]. This fast process produces a short window for the system to transfer energy to another emitter. The goal is to transfer the energy to an acceptor before the triplet state has time to emit light or is deactivated through non-radiative processes.

Both organic and inorganic acceptors have been attached to fluorene units to create systems designed for energy transfer. Copolymers containing lower band gap oligomeric segments[25], sensing units for metal ions[26] and red-emitting benzothiadiazoles[23] have been linked along with fluorene in a backbone. Ego et al.[27] fused polyfluorene with perylene dyes to achieve color tuning in the lower energy region of the visible spectrum. Tirapattur et al.[28] synthesized oligomeric segments of terfluorene capped with polyesters to control interchain interactions. Shu et al.[29] not only modified fluorene units along the backbone at the 2 and 7

positions, but functionalized the 9 position with different moieties within the same polymer. Furthermore, the high degree of functionalization around the fluorene was not a deterrent sterically, but instead suppressed aggregation.

Inorganic complexes have also been used as energy acceptors from fluorene. The metal-centered luminescence is typically more resistant to photobleaching over time. Gong et al.[30] blended a termer of a bipyridine-based iridium complex and fluorene with donor copolymers to form a guest-host system. Porphyrin-based platinum complexes have also been used as dopants within polyfluorene to produce red-emitting devices centered on the platinum luminescence[31].

In a few examples of the literature, lanthanides have been used as efficient emitters when coupled with polymer donors. Polystyrene-based polymers have been functionalized with a quinolinone chromophore ((**1**), **Figure 9**), which transfers its energy to the trivalent terbium cation[32]. In this compound, the coordination of the terbium cation is not well controlled, nor is it well understood. The few carboxylate groups contained in the polymer backbone indicate poor protection from deactivation. The lifetimes in methanol for this complex, 1.101 ms and 0.522 ms, confirm this indication. These values are far below that of $Tb(NO_3)_3$ in DMSO, for instance (2.61 ms)[2]. Europium complexes have also been incorporated as acceptors into polymers[33], [34] ((**2**) and (**3**), **Figure 9**). These systems blended the complexes with polymers with little control on the location or proximity of the host and guest. Ling et al.[35] ((**4**), **Figure 9**) synthesized a well-defined alternating copolymer containing fluorene used to donate energy to a europium complex, which subsequently emitted through the europium cation. However, the attachment of the europium complex to the polymer occurs *after* the copolymerization of the fluorene and carboxyphenylene. The control of the attachment of the polymer donor to the lanthanide complex acceptor is not fully optimized.

Figure 9. Several lanthanide polymer complexes. [32], [33], [34], [35]

3.4   RATIONALE FOR THE DESIGN OF OUR OLIGOFLUORENE LIGANDS

The design of our lanthanide ligand brought together two components which are crucial for

lanthanide sensitization: a versatile chromophore with high quantum yield and a coordinating

moiety with several sites for functionalization. Firstly, the lanthanide coordinating group would

have to have some control in how it attaches to the chromophore. In DTPA, we found a

lanthanide binder that is readily available in its bisanhydride form. The two anhydride groups

could be opened by the appropriate nucleophiles providing a strong bond to a chromophore.

The attractiveness of fluorene as a chromophore, in addition to high quantum yield, lied

in its ability to form precisely defined oligomer units. As the length of the conjugated

oligofluorene, acting as a donor, increased, the energy of absorption decreased. The decreased

donor energy could possibly sensitize lanthanides with lower accepting levels. The functionality

of the 9 position on fluorene also allowed for controlled distance between the donor and

acceptor. Alkylating this position and subsequent attachment to the lanthanide binder provided a fixed distance between the two moieties. The assessment of the Förster model as a mechanism for energy transfer was made because there was a distance factor (Förster based on r^{-6}) in the system. In our design, two amine-terminated alkyl chains opened both the anhydrides in the DTPA bisanhydride, which created a cavity accommodating the coordination of the lanthanide cation. Monofluorene and terfluorene ligands, both with the DTPA coordinating groups, were synthesized. Multiple lanthanide complexes with the three ligands were also prepared.

4.0   EXPERIMENTAL

4.1   CHEMICALS

All chemicals were used as received, unless otherwise specified. $Ln(NO_3)_3 \cdot 6H_2O$ (Ln = Eu, Gd, 99.99%) was purchased from Alfa Aesar. $Tb(NO_3)_3 \cdot 5H_2O$ (99.9%) diethylenetriamine-pentaacetic acid (DTPA, 98%) and triethylamine (99.5%) were purchased from Aldrich. Acetic anhydride (99.9%) was purchased from JT Baker. Butylamine (Aldrich, 99.5%) was dried over CaH_2. All NMR solvents were purchased from Cambridge Isotope Laboratories, Inc. and used as received. The internal standard for D_2O NMR samples, 3-(trimethylsilyl)propionic-2,2,3,3-d_4 acid, sodium salt (Aldrich, 98% D), was also used as received.

4.2   PHYSICAL MEASUREMENTS

NMR spectra were recorded using a Bruker DPX-300 (^{1}H: 300 MHz; ^{13}C: 75 MHz). Absorption spectra were collected on a Perkin-Elmer Lambda 9 spectro- photometer. Steady-state excitation and emission spectra were recorded at room temperature on a modified Jobin-Yvon Spex Fluorolog-322 spectrofluorimeter. Time-resolved excitation and emission spectra were recorded using a Varian Cary Eclipse coupled with a personal computer equipped with software supplied by Varian. Triplet state measurements were performed on the Varian Cary Eclipse using a cryostat apparatus manufactured by JY Spex and cooled with $N_{2(l)}$. Lanthanide luminescence

quantum yields were measured on the JY Spex Fluorolog-322 spectrofluorimeter using a Tb(2-hydroxyisophthalamide macrobicycle) complex in water (Φ=0.59)[4]. The quantum yields were calculated using the equation below:

$$\Phi_x/\Phi_r = [A_r(\lambda_r)/A_x(\lambda_x)][I(\lambda_r)/I(\lambda_x)][\eta_x^2/\eta_r^2][D_x/D_r]$$

where subscript r stands for reference and x for the sample; A is the absorbance at the excitation wavelength, I is the intensity of the excitation light at that same wavelength, η is the refractive index of the solvent (η = 1.333 H_2O; η = 1.479 DMSO; η = 1.4241 CH_2Cl_2) and D is the measured integrated luminescence intensity.

The luminescence lifetimes, centered on the respective metal's luminescence, were performed using a NdYAG Continuum Powerlite 8010 Laser (354 nm: 3rd harmonic; 266 nm: 4th harmonic) as the excitation source. Emission was collected at a right angle to the excitation beam and emission wavelengths were selected using a Spectral Products CM 110 1/8 meter monochromator (with two independent gratings). The signal was monitored by a Hamamatsu R928 photomultiplier coupled with a 500 MHz bandpass digital oscilloscope (Tektronix TDS 620B). The signals (50,000 points collected each trace) from at least 500 flashed were collected and averaged. Averaged luminescence lifetime values were obtained from three independent determinations. Luminescence decay curves were imported into Origin 7.0 scientific data analysis software. The decay curves were analyzed using the Advanced Fitting Tool module. The decay curves were fitted in mono-, bi- and tri-exponential modes. Of the three modes, the lifetime value was chosen based on the best fit of the decay curve on the criteria of the minimum χ^2 statistical parameter.

4.3   SYNTHESIS OF FLUORENE LIGANDS AND COMPLEXES
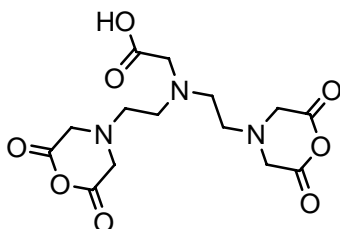
Diethylenetriaminepentaacetic acid bisanhydride (DTPA bisanhydride)   (1): According to

the method of Prudencio[36], DTPA (24.5 g, 62 mmol) was suspended in dry pyridine (31 mL)

and acetic anhydride (26.5 mL, 275 mmol) and stirred at 65°C for 24 h. The flask was cooled to

RT and the precipitate was collected, and then washed with copious amounts of diethyl ether.

The solid was dried under vacuum overnight to produce the title compound as a beige powder

(20.4 g, 57 mmol, 92%). ^{1}H NMR (DMSO-d_6, 300 MHz): δ 2.64 (t, 2H), 2.72 (t, 2H), 2.80 (t,

2H), 2.89 (s, 2H), 3.11 (t, 2H), 3.49 (s, 4H), 3.75 (s, 4H), 12.31 (s, 2H), ^{13}C NMR (DMSO-d_6, 75

MHz): δ 51.6, 52.7, 53.5, 55.5, 166.8, 172.9.

DTPA-bis(butylamide): Adapting the methods of Konings[37] and Gulgas[38], **(1)** (0.75 g, 2.10 mmol) was dissolved in 7.5 mL dry DMF under an $N_{2(g)}$ purge. In a separate flask, dry butylamine (0.46 mL, 4.5 mmol) was dissolved in 7.5 mL dry DMF and 2.5 mL triethylamine, also under an $N_{2(g)}$ purge. The butylamine solution was swiftly injected into the flask containing the DMF solution of **(1)**. The orange solution was stirred for 34 h under $N_{2(g)}$. The solvent was removed under vacuum, leaving a dark yellow residue. The residue was suspended in 8 mL water and the pH of the suspension was adjusted to 2.5 with concentrated HCl. The crude white crystals that form were collected and washed with cold ethanol. The crude crystals were dissolved in warm ethanol. The colorless crystals that formed were collected and dried (0.617 g, 1.22 mmol, 59 %). ^{1}H NMR (300 MHz, D_2O): δ 0.88 (t, 6H), 1.32 (m, 4H), 1.49 (m, 4H), 3.26 (m, 8H), 3.39 (m, 4H), 3.69 (s, 2H), 3.75 (s, 4H), 3.88 (s, 4H).

TF1 **(2):** In a variation to the methods of Konings[37] and Gulgas[38], diamino terfluorene (8.9 mg, 9 μmol, **Figure A1**) and **(1)** (3.1 mg, 9 μmol) were dissolved in 1 mL DMF under an $N_{2(g)}$ purge. 10 μL triethylamine was added via syringe to the stirring solution. The capped solution was stirred under nitrogen for 30 h. The solvent was removed in vacuo. The remaining residue was suspended in 5 mL water and the pH is adjusted to 11.4 with dilute $NaOH_{(aq)}$. The aqueous layer was washed with diethyl ether and methylene chloride to remove excess base and unreacted terfluorene. The aqueous layer was adjusted to pH 2.5 with dilute HCl, at which point a sticky solid precipitate formed. The water was removed in vacuo, yielding 16 mg. ^{1}H NMR (300 MHz, DMSO-d_6): 0.31-0.75 (br, 24H), 0.75-1.15 (br, 36H), 1.75-2.30 (br, 16H), 3.00-4.58 (br, 160H), 7.20-7.50 (br, 6H), 7.58-8.09 (br, 14H).

Preparation of Lanthanide Complexes [from MF1 (**Figure 10**), MF2 (**Figure 18**) and TF1 (**Figure 25**) ligands, respectively]

To a dilute solution of 11 μmol oligofluorene ligand in DMSO, 11 μmol of $Ln(NO_3)_3 \cdot xH_2O$ was added with stirring. After 2 h, 17 μmol Na_2CO_3 was added to the stirring solution. This solution stirred for an additional 24 h and solvent was removed and dried in vacuo to yield the lanthanide complexes $MF1:Eu^{3+}$, $MF1:Tb^{3+}$, $MF1:Gd^{3+}$, $MF2:Eu^{3+}$, $MF2:Tb^{3+}$, $MF2:Gd^{3+}$, $TF1:Eu^{3+}$, $TF1:Tb^{3+}$ and $TF1:Gd^{3+}$.

5.0   RESULTS AND DISCUSSION – MONOFLUORENE COMPLEXES

5.1   SYNTHESIS OF THE MONOFLUORENE (MF1) LANTHANIDE COMPLEXES

The monofluorene ligand with pendant butenyl arms (MF1), the fluorene moiety connected to the DTPA coordinating group (**Figure 10**), was received as a fully characterized product from Dr. James Copenhafer of the Meyer group. The fluorene served as the lanthanide antenna, the moiety which harvested light and transferred the energy to the lanthanide cation.
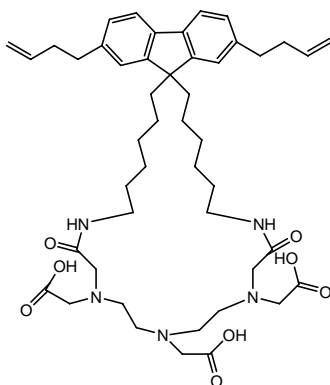
Figure 10. The monofluorene ligand with butenyl arms (MF1).

The ligand contained a well-defined coordination site for a lanthanide cation: a large cavity with peripheral amide bonds, nitrogen atoms and dangling carboxylic acid arms. When the acid groups were deprotonated they became hard Lewis bases and formed strong bonds with hard Lewis acids, such as trivalent lanthanide cations. The resonance structure of the carboxylate group upon coordination to a metal ion is displayed in **Figure 11**. Several of these coordinating

carboxylate groups were needed to complete the lanthanide coordination requirements. The DTPA moiety provided three carboxylate arms for coordination to the lanthanide cation.
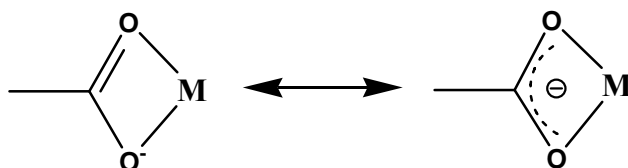
Figure 11. Coordination to a metal ion and the resonance of the carboxylate group.

Coordination of the lanthanide cations to these ligands was performed by deprotonating the carboxylic acid groups of the ligand with a carbonate base, CO_3^{2-}, in the presence of lanthanide nitrate in a DMSO solution. The lanthanide complexes were collected after solvent removal and dried to isolate.

Europium and terbium were chosen as the lanthanides for the formation of luminescent complexes emitting in the visible because they have accepting electronic level energies compatible with the donating energy of the triplet states of the MF1 ligand. Furthermore, the emission intensities of several transitions of Eu^{3+} and Tb^{3+} are known to vary depending on the environments around these cations[2]. Eu^{3+} has a unique transition ($^5D_0 \rightarrow {^7F_0}$) that can be used to probe the coordination geometry around the lanthanide cations in the coordination complexes. Ling et al.[35] reported that lanthanide cations could be sensitized by conjugated systems, such as polyfluorene. Their fluorene-phenylene copolymers used the copolymer backbone as a chromophore, transferring energy to a europium complex coordinated to the phenylene monomer. They tuned the triplet state of the donor to the accepting level of the lanthanide cation by coordinating several β-diketone ligands to the lanthanide cation. This differed from our approach in that we used discrete lengths of oligofluorene in tuning the donating energy levels.

5.1.1 PHOTOPHYSICAL PROPERTIES

The goal of this part of the project was to determine whether the fluorene acted as a suitable antenna by harvesting light and effectively transferring its energy to the accepting level of the lanthanides to obtain luminescent complexes. Luminescence spectra allowed us to assess the presence of ligand to lanthanide energy transfer in these systems. In the MF1 Tb^{3+} and Eu^{3+} complexes, simultaneous steady-state emission bands arising from both the fluorene and the respective lanthanides were observed. The presence of lanthanide emission, upon fluorene excitation, in steady-state mode indicated that the fluorene transferred energy to the accepting levels of the lanthanides. These steady-state spectra of the $MF1:Tb^{3+}$ and $MF1:Eu^{3+}$ complexes are depicted in **Figures 12** and **13**, respectively. The sharp lanthanide emission bands were observed at 490 nm ($^5D_4 \rightarrow {}^7F_6$) and 545 nm ($^5D_4 \rightarrow {}^7F_5$) in the spectrum of **Figure 12** for the terbium complex. In **Figure 13**, the 614 nm ($^5D_0 \rightarrow {}^7F_2$) emission band was observed for Eu^{3+}. The insets displayed in **Figures 12** and **13** show the expanded lanthanide-centered emission bands, respectively, and were obtained using the same excitation wavelength (278 nm), corresponding to excitation through the fluorene electronic levels. This excitation band was observed on both absorption and excitation spectra in **Figures 12** and **13** for the Tb^{3+} and Eu^{3+} complexes, respectively. Using the same excitation wavelength for both Tb^{3+} and Eu^{3+} complexes indicated that the lanthanide emission was obtained through the electronic levels centered on the monofluorene moiety.

Table 1. Luminescence lifetimes centered on the lanthanide excited states and quantum yields for the MF1 complexes (~10^{-6} M in DMSO), 298 K.

Sample Complex	Lifetimes (λ_{em}, transition) (ms)[b]	Quantum Yield[a,c]
MF1:Tb^{3+}	2.32 ± 0.03 1.5 ± 0.3 (545 nm, $^5D_4 \rightarrow {}^7F_5$)	0.029 ± 0.006
MF1:Eu^{3+}	1.36 ± 0.01 0.40 ± 0.05 (614 nm, $^5D_0 \rightarrow {}^7F_2$)	0.019 ± 0.003

a. Quantum yield measurements using TbH22IAM[4] in water as a reference ($\Phi = 0.59$).
b. $\lambda_{ex} = 354$ nm.
c. $\lambda_{ex} = 315$ nm.

The efficiency of the fluorene to lanthanide energy transfer and the quenching of the lanthanide excited states were quantified through quantum yields measurements of the complexes upon fluorene excitation, monitoring the lanthanide emission. These values were measured relative to a terbium 2-hydroxyisophthalamide complex in water ($\Phi = 0.59$)[4]. The results are reported in **Table 1**. The higher value of the terbium complex quantum yield (0.029 ± 0.006) is explained by a lower susceptibility to deactivation from the excited states of the complex, such as the triplet state donating level of the monofluorene or the accepting level ($^5D_4$, 20, 545 cm^{-1}) of the Tb^{3+}. By comparison, the deactivation in the MF1:Eu^{3+} complex was greater, resulting in a smaller quantum yield value (0.019 ± 0.003). The tuning of the donating energy levels to the accepting levels of Eu^{3+} ($^5D_{1,0}$) was probably less effective in the MF1:Eu^{3+} complex, relative to MF1:Tb^{3+}, as well. Nonetheless, such values are comparable to quantum yields reported for complexes used in commercial bioanalytical applications. For example, Lehn europium cryptate complexes (Eu(bpy:bpy:bpy)), commercially available as fluoroimmuno-assays, have quantum yields of about 2-3 %[39]. These quantum yield values indicate that the

efficiency of the ligand to lanthanide energy transfer in these MF1 complexes was small, and/or that a quenching process deactivated the lanthanide excited state.

The fluorene steady-state emission was the most intense signal at ~358 nm in the emission spectra of these complexes (**Figures 12** and **13**). The steady-state emission of the fluorene, in both MF1 Tb^{3+} and Eu^{3+} complexes, appeared as two bands and one shoulder band[16]. All of these bands were attributed to fluorene-centered π-π* singlet states.
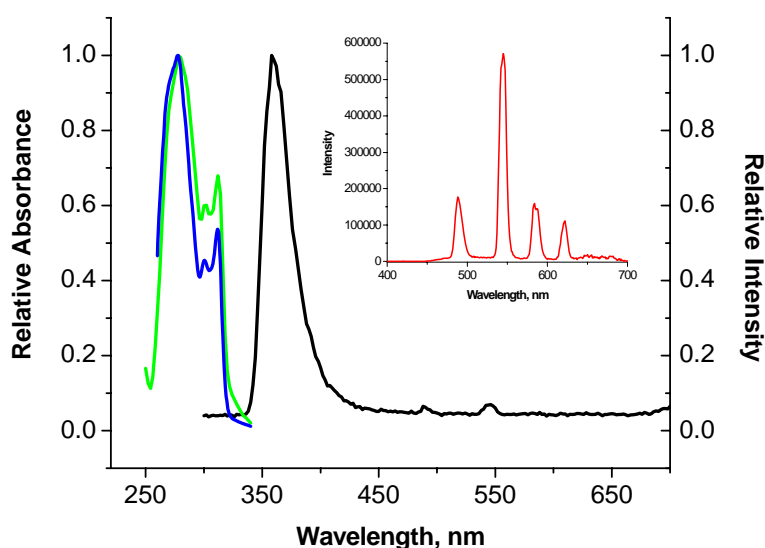
Figure 12. Relative absorbance (blue), steady-state excitation (green, λ_{em} = 357 nm) and emission (black, λ_{ex} = 278 nm) spectra for MF1:Tb^{3+} complex (~10^{-6} M) in DMSO, 298 K. Inset: The same sample, collected under different instrumental conditions to allow for more detailed monitoring of the lanthanide emission signal. This displays the sharp emission bands arising from Tb^{3+}.
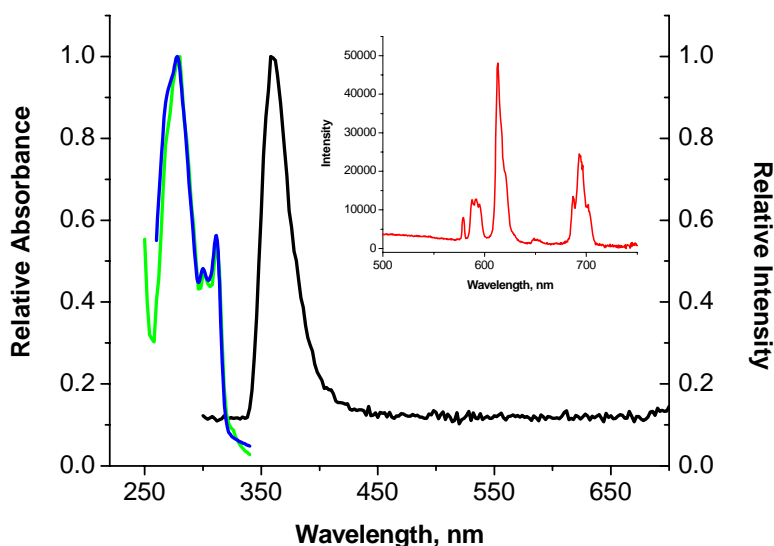
Figure 13. Relative absorbance (blue), steady-state excitation (green, λ_{em} = 360 nm) and emission (black, λ_{ex} = 278 nm) spectra for MF1:Eu^{3+} complex (~10^{-6} M) in DMSO, 298 K. Inset: The same sample, collected under different instrumental conditions to allow for more detailed monitoring of the lanthanide emission signal. This displays the sharp emission bands arising from Eu^{3+}.

From the steady-state emission spectra, we have demonstrated that MF1 sensitizes both Tb^{3+} and Eu^{3+}. In time-resolved excitation spectra, the band resulting from the antennae can usually be discriminated because its band(s) are broader than the atom-like excitation bands centered on the lanthanide cations. Such time-resolved spectra helped confirm the antenna effect provided by the MF1 complexes.

The time-resolved emission spectra of the respective complexes in DMSO are depicted (**Figure 14**: MF1:Tb^{3+} complex; **Figure 15**: MF1:Eu^{3+} complex). The sharp emission bands, characteristic of the respective lanthanide cations, were at similar energy positions for the spectra in the respective complexes.
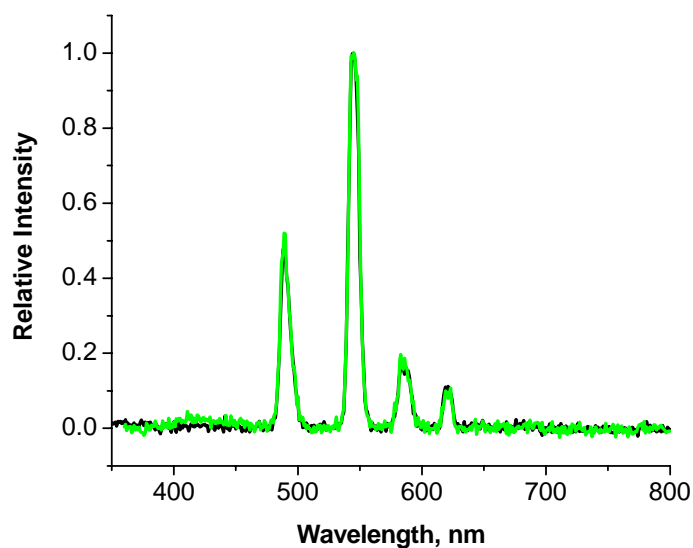
Figure 14. Normalized time-resolved emission spectra of MF1:Tb^{3+} complex (~10^{-6} M) in DMSO, 298 K. λ_{ex} = 331 nm (black), 352 nm (green, direct excitation).
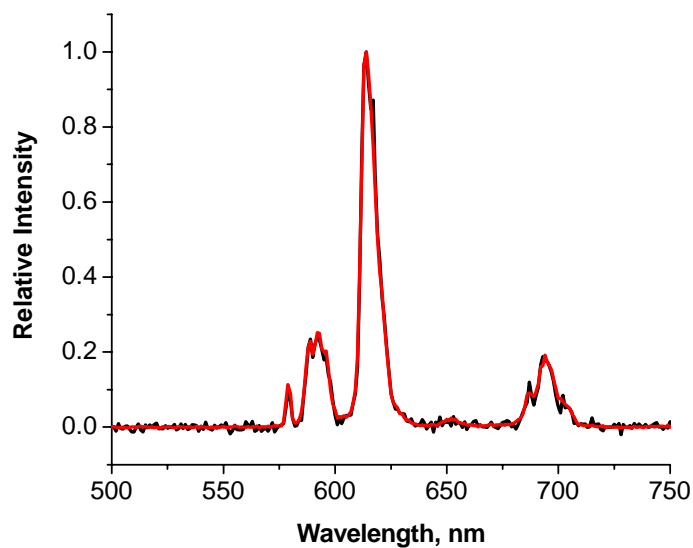
Figure 15. Time-resolved emission spectra (normalized) of MF1:Eu^{3+} complex (~10^{-6} M) in DMSO, 298 K. λ_{ex} = 329 nm (black), 395 nm (red, direct excitation).

The time-resolved excitation spectra of the MF1:Tb^{3+} complex in DMSO is depicted in

Figure 16 (black line). The broad band, whose maximum appeared at 331 nm, was attributed to

the MF1 ligand because it was also present at the same energy on the time-resolved excitation

spectrum of the MF1:Eu^{3+} complex (**Figure 17**, black line). This common, broad excitation band

did not appear in the steady-state excitation and absorption spectra of either the Tb^{3+} or Eu^{3+}

complexes (**Figures 12** and **13**). This band may have resulted from a triplet state, which may

have been covered by the more intense band arising from the singlet states of the fluorene in

steady-state mode.

Figure 16. Normalized time-resolved excitation spectra of MF1:Tb^{3+} complex (black, ~10^{-6} M) and Tb(NO$_3$)$_3$ (green, 10 mM), both in DMSO, 298 K. λ_{em} = 545 nm.

The antenna effect was evidenced by this broad band centered at ~330 nm for both Tb^{3+}

and Eu^{3+} complexes. These time-resolved excitation spectra also contained sharper bands that are

due to the direct excitation of the excited states of the respective lanthanide cations. The time-

resolved excitation spectrum of a free lanthanide cation, Tb(NO$_3$)$_3$, in DMSO (**Figure 16**, green)

is displayed as a reference on the same plot that contains the terbium complex spectrum. The

sharp excitation bands corresponded to the direct excitation of the excited electronic levels of

Tb^{3+} and appeared at the same energy position in both spectra. The strong resemblance of the

spectra in **Figure 16**, with the presence of sharp excitation bands in both cases, indicated that

most of the Tb^{3+} excitation occurred directly through its own levels and that the antenna effect in

the MF1:Tb^{3+} complex was weak. The time-resolved excitation spectrum of the MF1:Eu^{3+}

complex in DMSO is shown in **Figure 17**. The common, broader excitation band at 329 nm was

indicative of the MF1 ligand acting as an antenna and transferring some energy to the europium

cation. The time-resolved excitation spectrum of $Eu(NO_3)_3$ in DMSO (**Figure 17,** red) also

exhibited a series of sharp, direct excitation bands centered on Eu^{3+}. The sharp excitation bands

of the free Eu^{3+} cation were located at the same energies as the sharp excitation bands in the

europium MF1 complex. As with the terbium complex, the majority of the spectrum contained

the sharp, direction excitation bands of Eu^{3+}, indicating the antenna effect was also weak in the

MF1:Eu^{3+} complex. The luminescence spectra helped us build a complete picture of the energies

of different excited states present in the MF1 complexes (see Chapter 7).
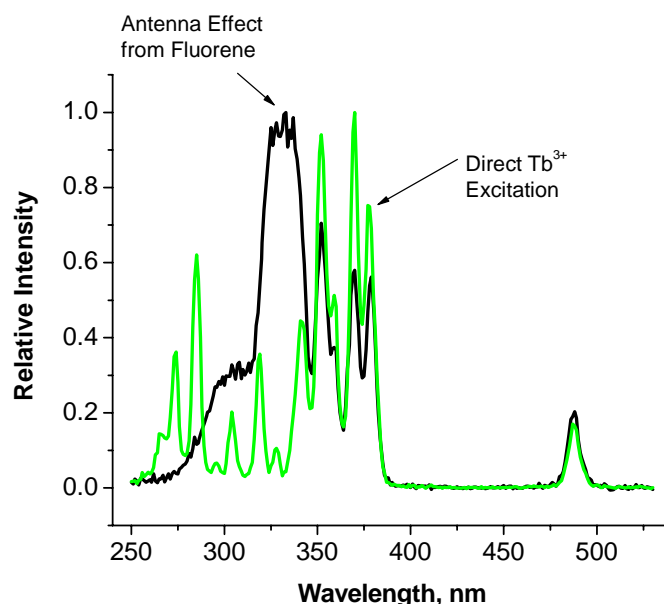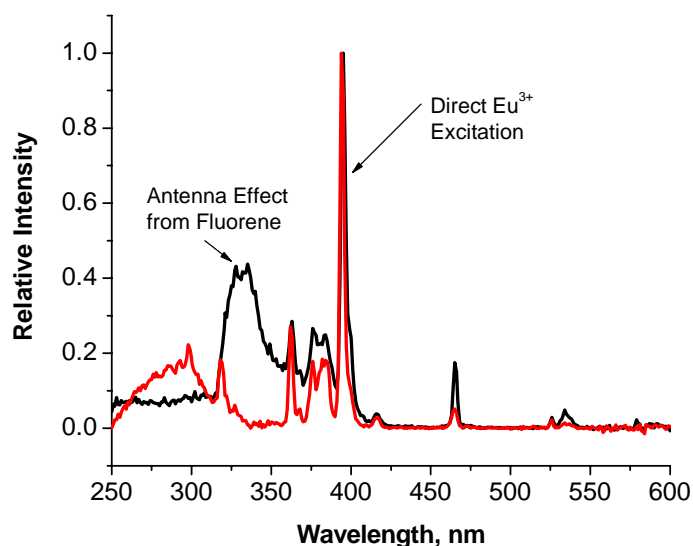

Figure 17. Normalized time-resolved excitation spectra of MF1:Eu^{3+} complex (black, ~10^{-6} M) and $Eu(NO_3)_3$ (red, 10 mM), both in DMSO, 298 K. λ_{em} = 614 nm.

5.1.2 LUMINESCENCE LIFETIME MEASUREMENTS (LANTHANIDE-CENTERED EMISSION, 298 K)

Luminescence lifetimes of the lanthanide excited states in the respective complexes recorded upon ligand excitation are reported in **Table 1**. The lifetimes were an indicator of how well the ligand protected the lanthanide cation. The experimental exponential decay fit best as a bi-exponential. Two values were obtained for both the terbium and europium complexes and were indicative of two different lanthanide environments. For one environment, the lanthanide cation was well protected from any source of deactivation in its surroundings. This lanthanide cation had a longer luminescence lifetime[2]. In comparison to other lanthanide complexes, the longer component lifetime of our respective complexes suggested a well-protected lanthanide cation[40]. The shorter lifetime component recorded for each complex indicated an environment where the lanthanide cations were less protected from non-radiative deactivation. Gulgas and Reineke calculated one water molecule coordinated to the lanthanide cation in their macrocyclic europium complexes[38]. These macrocyclic complexes also included the DTPA coordinating moiety. They reported an average lifetime of 0.7 ms in water for their Eu^{3+}-complex (mono-exponential fitting). The larger component lifetime of our monofluorene:Eu^{3+} complex was twice this value. The shorter lifetime component of our monofluorene:Eu^{3+} complex was approximately equal to half of their value (0.4 ms versus 0.7 ms).

30

5.2   SYNTHESIS OF THE MONOFLUORENE (MF2) LANTHANIDE COMPLEXES

The monofluorene ligand MF2 (**Figure 18**) was received as a fully characterized product from

Rob Walters of the Meyer group. The architecture of MF2 is similar to that of MF1 with the

absence of the pendant butenyl "wings". MF2 contained a single fluorene unit, which served as

the light-harvesting chromophore, and a DTPA moiety. The DTPA acted as the coordinator of

the lanthanide cation.
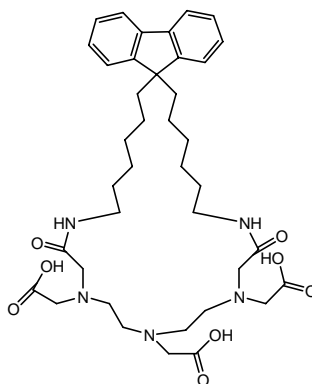
Figure 18. The second monofluorene ligand (MF2).

The butenyl wings on the fluorene backbone of MF1 served as precursors for ADMET

(acyclic diene metathesis) polymerization[41]. The purpose for removing these wings in the MF2

was to resemble the TF1 ligand, which was synthesized without the pendant wings. This allowed

for a more direct comparison of the two chromophores in the MF2 and TF1 ligands. The

influence of the conjugation in the wings was assessed through a comparison of the

photophysical properties of MF1 and MF2. The carbonate anion, CO_3^{2-}, was used as the base to

deprotonate the carboxylic acid groups about the DTPA moiety of the MF2 ligand. The

lanthanide complexes were subsequent formed in the presence of lanthanide nitrate in DMSO. Solid precipitate was collected and dried to isolate the lanthanide complexes.

Europium and terbium were chosen as the luminescent lanthanide cations for complexation because the energies of their accepting levels (Tb^{3+}: $^5D_4$; Eu^{3+}: $^5D_1$, $^5D_0$) are compatible with the donating energy levels of the MF2 ligand. A gadolinium complex of MF2 was also synthesized to monitor the photophysical characteristics of the ligand in the presence of a spectroscopically silent lanthanide cation. Triplet state information was also acquired with measurements on the MF2:Gd^{3+} complex (Chapter 7).

5.2.1 PHOTOPHYSICAL PROPERTIES

The goal of this part of the project was to assess the MF2 ligand as a viable antenna for the luminescent lanthanide cations, Eu^{3+} and Tb^{3+}. The luminescence spectra of the MF2 lanthanide complexes allowed us to qualitatively determine the extent of ligand to lanthanide energy transfer. **Figures 19** and **20** depict the absorption and steady-state spectra of the MF2:Eu^{3+} and MF2:Tb^{3+} complexes in DMSO, respectively. The broad fluorene band (360 nm) and respective lanthanide emission bands simultaneously appear, upon ligand excitation, in the steady-state emission spectra (λ_{ex} = 304 nm) for both complexes. In each spectrum, the lanthanide emission bands were well-resolved and characteristically sharp. In **Figure 19**, the emission bands for europium were observed at 579 nm ($^5D_0 \rightarrow {}^7F_0$), 593 nm ($^5D_0 \rightarrow {}^7F_1$), 613 nm ($^5D_0 \rightarrow {}^7F_2$), 651 nm ($^5D_0 \rightarrow {}^7F_3$) and 695 nm ($^5D_0 \rightarrow {}^7F_4$). The observation of the well-resolved emission of europium in the steady-state mode indicated that the ligand to lanthanide energy transfer is present. Indeed, the quantum yield centered on the luminescence of Eu^{3+} in the MF2:Eu^{3+} complex in DMSO was 1.0 ± 0.2% (**Table 2**), using the terbium 2-hydroxyisophthalamide

complex in water ($\Phi = 0.59$) as a reference[4]. However, the presence of fluorene ligand emission

signified the ligand to lanthanide energy transfer is incomplete.

Figure 19. Relative absorbance (green), steady-state excitation (blue, λ_{em} = 360 nm; red, λ_{em} = 614 nm) and emission (black, λ_{ex} = 304 nm) spectra for MF2:Eu^{3+} complex (~10^{-6} M) in DMSO, 298 K. The transitions of emission for Eu^{3+} are also labeled in black.

The steady-state excitation spectra in **Figure 19** have emission wavelengths at the

monofluorene ligand (λ_{em} = 360 nm, green) and Eu^{3+} cation (λ_{em} = 614 nm, red). The excitation

bands overlapped completely. Strong resemblance of the emission bands in the two spectra

indicated that the lanthanide emission was sensitized through the fluorene ligand and not excited

directly through Eu^{3+}. Furthermore, the excellent overlap of the excitation bands with the

absorption spectrum (blue) indicated the excitation of the ligand, followed by subsequent

emission through the fluorene and europium, was accessed through electronic levels centered on

the ligand.

Table 2. Luminescence lifetimes centered on the lanthanide excited states and quantum yields for the MF2 complexes (80 µM in DMSO), 298 K.

Sample Complex	Lifetimes (λ_{em}, transition) (ms)[b]	Quantum Yield[a,c]
MF2:Eu^{3+}	1.44 ± 0.01 0.51 ± 0.03 (614 nm, $^5D_0 \rightarrow {}^7F_2$)	0.010 ± 0.002
MF2:Tb^{3+}	2.45 ± 0.02 1.06 ± 0.02 (545 nm, $^5D_4 \rightarrow {}^7F_5$)	0.044 ± 0.005

a. Quantum yield measurements using TbH22IAM[4] in water as a reference (Φ=0.59).
b. $\lambda_{ex} = 266$ nm.
c. $\lambda_{ex} = 305$ nm.

The simultaneous emission bands arose from the monofluorene (360 nm) and terbium in the steady-state emission spectrum ($\lambda_{ex} = 304$ nm) of MF2:Tb^{3+} in DMSO (**Figure 20**, black). The terbium emission was observed at 489 nm ($^5D_4 \rightarrow {}^7F_6$), 545 nm ($^5D_4 \rightarrow {}^7F_5$), 583 nm ($^5D_4 \rightarrow {}^7F_4$), 621 nm ($^5D_4 \rightarrow {}^7F_3$) and 651 nm ($^5D_4 \rightarrow {}^7F_2$). The sharp emission bands of terbium occurred in the steady-state mode, indicative of good ligand to lanthanide energy transfer. Moreover, the terbium emission bands were intense relative to the emissive signal of the fluorene at 360 nm. The high quantum yield ($4.4 \pm 0.5\%$), centered on terbium (**Table 2**), was reflective of the favorable energy transfer suggested in the steady-state emission spectrum. Measurement of the quantum yield of the MF2:Tb^{3+} complex in DMSO also used the terbium 2-hydroxy-isophthalamide complex in water as a reference.

The steady-state excitation spectra in **Figure 20** have emission wavelengths at the monofluorene ligand ($\lambda_{em} = 360$ nm, green) and Tb^{3+} cation ($\lambda_{em} = 545$ nm, red), and they overlapped completely. The similarity in the bands of the two excitation spectra indicated that the lanthanide emission was sensitized through the fluorene ligand and not excited directly through Tb^{3+}. Furthermore, the simultaneous steady-state emission of the fluorene and terbium was supported by the large overlap of the absorption spectrum (**Figure 20**, blue) with the

excitation spectra for MF2:Tb^{3+}. This overlap meant, as with the MF2:Eu^{3+} complex, that the excitation of the ligand, followed by energy transfer, was accessed through electronic levels centered on the fluorene antenna. The antenna effect held true for both of the MF2 lanthanide complexes.
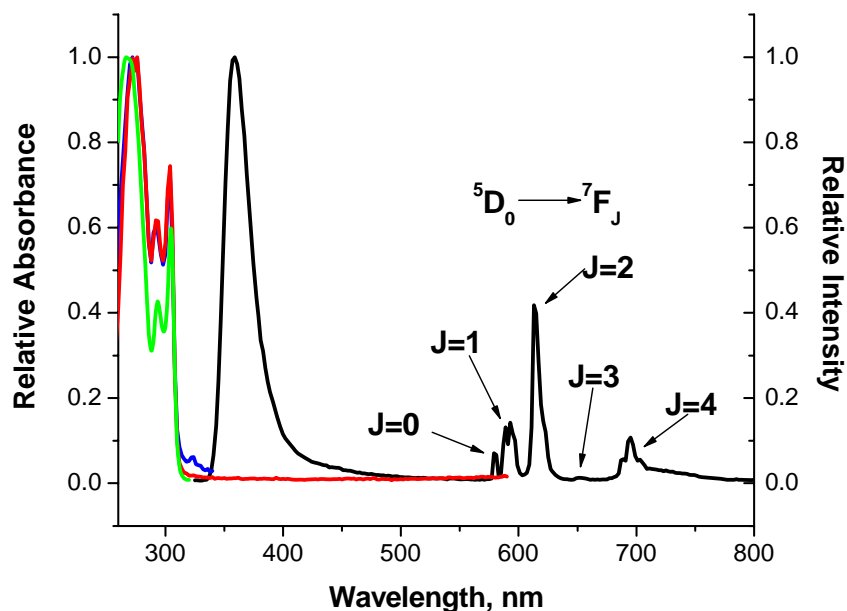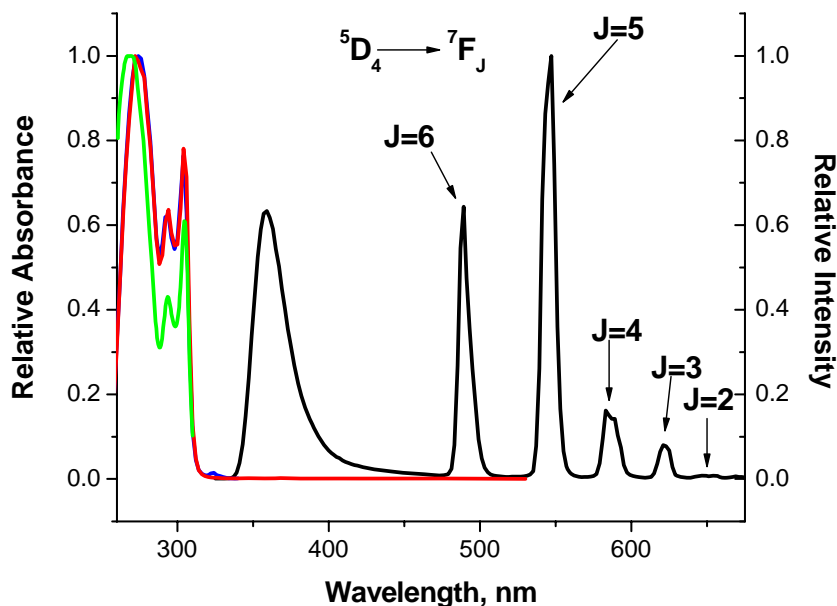

Figure 20. **Relative absorbance (green), steady-state excitation (blue, λ_{em} = 360 nm; red, λ_{em} = 545 nm) and emission (black, λ_{ex} = 304 nm) spectra for MF2:Tb^{3+} complex (~10^{-6} M) in DMSO, 298 K. The transitions of emission for Tb^{3+} are also labeled in black.**

The high quantum yield values for the MF2 lanthanide complexes indicated a small amount of efficiency was attained in these systems. The MF2:Eu^{3+} and MF2:Tb^{3+} complexes in DMSO are also comparable to commercially available fluoroimmunoassays currently available that utilize lanthanide emission (Chapter 5.1.1).

Steady-state and absorption spectra for MF2:Gd^{3+} in DMSO is displayed in **Figure 21**. The fluorene emission spectrum (black, λ_{ex} = 304 nm) contained the same broad fluorene band at 360 nm as the luminescent lanthanide MF2 complexes. The excitation and absorption spectra profiles also were similar in energy to the MF2:Eu^{3+} and MF2:Tb^{3+} complexes. Their similarity

further supported the claim that the antenna effect was occurring from the fluorene to the luminescent lanthanide cations because the energy was accessed through the same fluorene electronic levels.
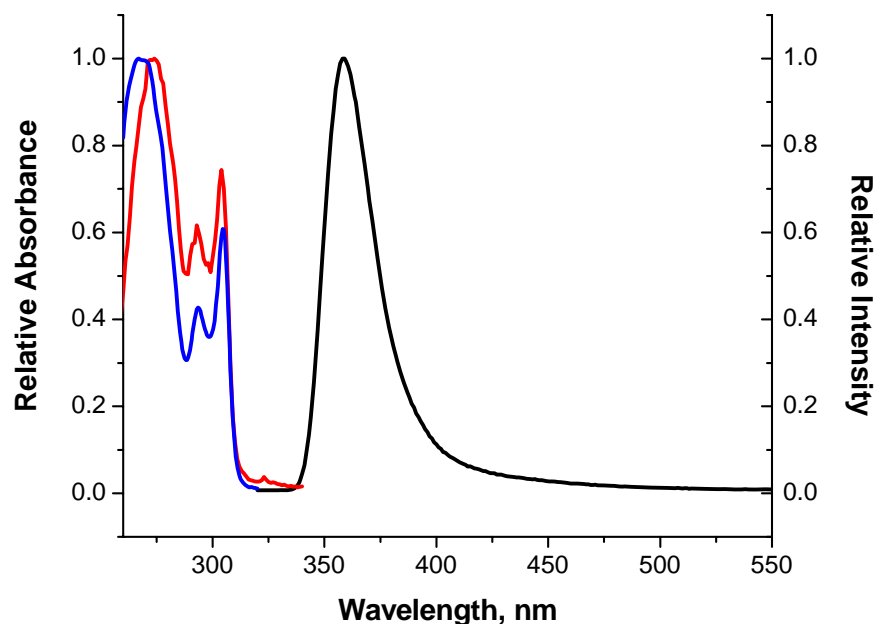
Figure 21. Relative absorbance (blue), steady-state excitation (red, λ_{em} = 360 nm) and emission (black, λ_{ex} = 304 nm) spectra for MF2:Gd^{3+} complex (~10^{-6} M) in DMSO, 298 K.

5.2.2 LUMINESCENCE LIFETIME MEASUREMENTS (LANTHANIDE-CENTERED EMISSION, 298 K)

The luminescence lifetimes of the lanthanide excited states, measured upon ligand (MF2) excitation, is reported in **Table 2**. The lifetime values served as a good indication of how well the ligand protected the lanthanide cation. In both the MF2:Eu^{3+} and MF2:Tb^{3+} complexes in DMSO, the luminescence decay fit best as a bi-exponential function. The two different lifetime values for each of the respective complexes represented two unique lanthanide cation environments. The longer lifetime component was consistent with a well-protected lanthanide cation environment. The longer component was less susceptible to non-radiative deactivation

36

such as solvent quenching. A well-protected lanthanide cation has a longer luminescence lifetime. Each set of lifetime values also contained a shorter component. This shorter lifetime was indicative of a lanthanide environment which was less protected from deactivation. The long lifetime component in the respective MF2 complexes was comparable to lifetimes found in other lanthanide complexes. For instance, the long component of the MF2:Eu^{3+} complex in DMSO (1.44 ms) was significantly longer than the lifetime of Selvin's Eu-DTPA-cs124 in H_2O (0.62 ms)[40]. This further supported that there is adequate protection around at least one of the lanthanide cation environments in both of the MF2 complexes.

6.0   RESULTS AND DISCUSSION – TERFLUORENE COMPLEX

6.1   SYNTHESIS OF THE TERFLUORENE LIGAND (TF1) AND LANTHANIDE COMPLEXES

The terfluorene ligand (TF1) was synthesized to produce an oligofluorene antenna with lower singlet and triplet state energies, due to the extended conjugation of the three fluorene units. The attachment of amine-terminated alkyl group to the DTPA coordinating group was studied extensively before similar reactions on the terfluorene moiety were performed. The goal of this effort was to optimize the reaction of the nucleophilic amine opening the DTPA bisanhydride, resulting in amide bond formation. This work also revealed more about the large ligand cavity where lanthanide cation coordination occurred in our complexes. Konings et al.[37] synthesized DTPA-bis(ethylamide), with the goal of complexing gadolinium, in its acidic form (**Figure 22**). Gulgas and Reineke[38] synthesized macrocyclic DTPA-containing compounds with their intermediate products as sodium complexes (**Figure 22**). We synthesized DTPA-bis(butylamide) and attempted precipitation of the product both as an acid and sodium salt.
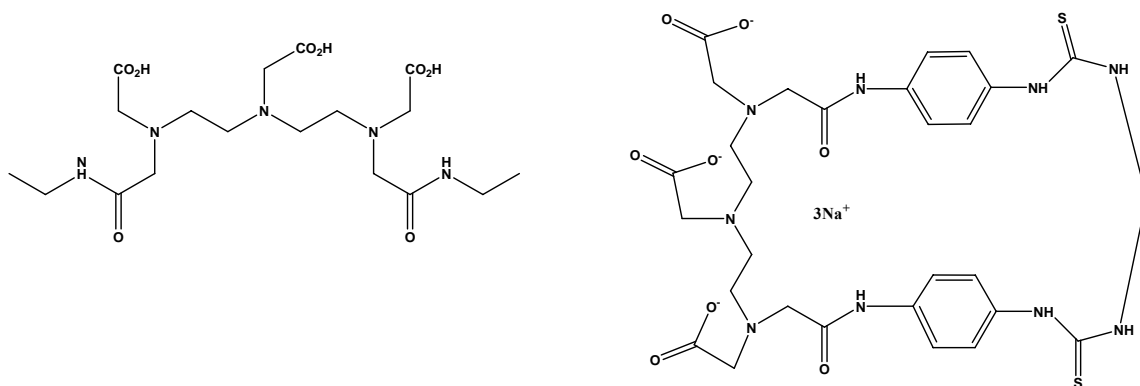
Figure 22. Molecules from the literature with DTPA coordinating groups. [37], [38]

Konings et al.[37] reported a characteristic fingerprint of the DTPA proton shifts in their

^{1}H NMR spectrum of DTPA-bis(ethylamide). We report this same pattern of shifts, displayed in

Figure 23 for DTPA-bis(butylamide). The 2:2:1:2:4 ratio of the peaks, from left to right,

represented the signature pattern of the DTPA protons for a doubly-substituted DTPA

bisanhydride.
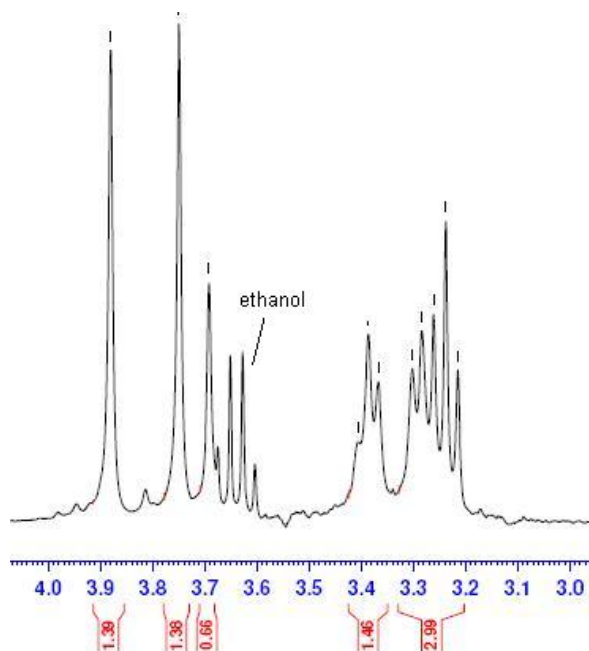
Figure 23. ^{1}H NMR spectrum of DTPA-bis(butylamide) in D₂O. The ratio of the peaks (left to right, excluding ethanol quartet) is 2:2:1:2:4, the signature of the DTPA protons.

When the DTPA-bis(butylamide) was precipitated as a sodium salt at basic pH (~11), the DTPA proton region of the spectrum (4.2 – 2.4 ppm) was not as well resolved. This was probably due to the bulkiness of Na^+ relative to a proton and the distortion it induced in the ^1H NMR spectrum. The acidic form of the product can crystallize more easily because the preferred conformation was not as sterically hindered by a large cation.

The terfluorene moiety, received as a fully characterized product from Dr. James Copenhafer, and DTPA bisanhydride were reacted in DMF under nitrogen with an appropriate amount of triethylamine as base. After solvent removal the pH of the product suspended in water was adjusted to 11 to deprotonate the reacted base. Subsequently, base and unreacted terfluorene were removed through extraction with diethyl ether. The aqueous layer was acidified to pH 2.5 and the water was removed. The ^1H NMR spectrum in DMSO-d_6 indicated broad methylene peaks upfield from the DTPA proton region, which were not well resolved (**Figure 24**).

Furthermore, the DTPA to fluorene methylene proton ratio was about 4:1, which was not indicative of one DTPA moiety attached to one terfluorene. The ratio of the DTPA to terfluorene may be 2:1 with one DTPA group attached to each terminal amine, instead of one DTPA bridging across the two terminal amines.
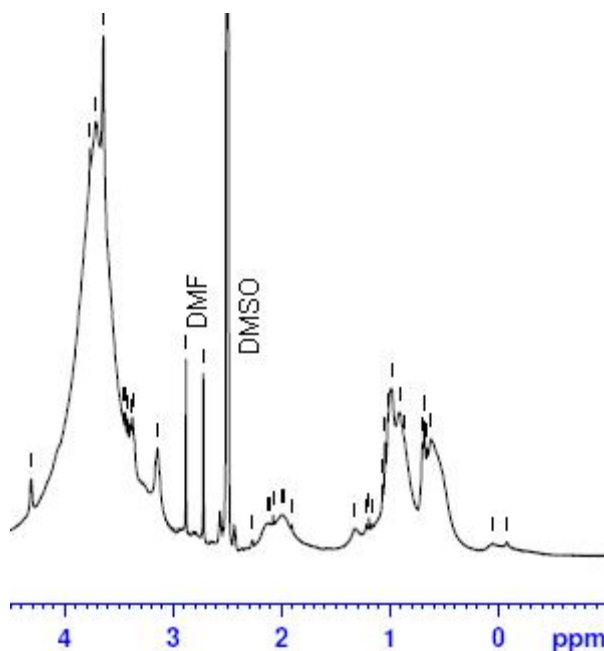
Figure 24. ^1H **NMR spectrum in DMSO-d_6 of the terfluorene ligand. The proton ratio of DTPA to fluorene methylenes is ~ 4:1.**

40

There was likely some excess of DTPA present in the aqueous layer after acidification because unreacted fluorene was removed in the extraction. These reasons could explain the increase in the total number of DTPA protons reported in the spectrum of **Figure 24**.

The lanthanide coordination to form the respective terfluorene complexes was performed in the same manner as the monofluorene ligand complexation. In DMSO, the lanthanide nitrate and TF1 (**Figure 25**) were stirred for 2 h. At this time, Na_2CO_3 was added to deprotonate the carboxylic acids and enable coordination of the lanthanide cations. After stirring overnight, the product was collected through solvent removal and dried to isolate the complex. Europium, terbium and gadolinium were chosen as the lanthanides for coordination. Eu and Tb formed luminescent lanthanide complexes emitting in the visible and their accepting levels should be compatible with the donating energies of TF1. The Gd^{3+} complex allowed us to obtain more information about the energies of the electronic levels in the terfluorene ligand in Chapter 7.
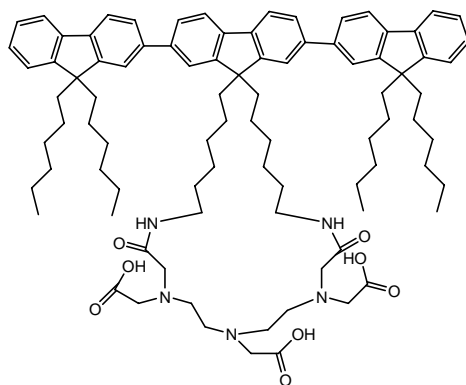
Figure 25. The terfluorene ligand (TF1).

6.2   PHOTOPHYSICAL PROPERTIES

The goal of this part of the project was to determine whether TF1 can collect light and efficiently transfer that energy to the accepting levels of Eu^{3+} and Tb^{3+}, forming a luminescent complex. Using the same analytical tools for photophysical characterization of the MF1 and MF2 complexes, we assessed the presence of energy transfer from the terfluorene to both Eu^{3+} and Tb^{3+} in these respective complexes. Intense steady-state fluorene emission was evident for both complexes; however, simultaneous, steady-state lanthanide emission was only present in the Eu^{3+} complex at 614 nm ($^5D_0 \rightarrow {}^7F_2$, **Figure 26**). In the **Figure 26** inset, the sharp, europium centered emission bands were obtained using the excitation wavelength (353 nm) corresponding to the terfluorene. The presence of steady-state lanthanide emission in the europium complex, upon excitation of the terfluorene, indicated that the terfluorene transferred energy to the accepting levels of the europium cation. There was no indication of efficient terfluorene to Tb^{3+} energy transfer in the terbium complex based on its steady-state emission spectrum (**Figure 27**).

Figure 26. Relative absorbance (blue), steady-state excitation (red: λ_{em} = 418 nm) and steady-state emission (black, λ_{ex} = 353 nm) of TF1:Eu^{3+} complex in CH$_2$Cl$_2$ (~10^{-6} M), 298 K. Inset: The same sample, collected under different instrumental conditions to allow for more detailed monitoring of the lanthanide emission signal. This displays the sharp emission bands arising from Eu^{3+}.

Terbium-centered emission bands <u>were not</u> observed in steady-state, despite excitation through

the terfluorene at the same wavelength (353 nm) as the europium complex. Similar shapes of the

absorption and excitation spectra for both complexes indicated that steady-state emission is

obtained via the electronic level of the terfluorene. However, the energy was not transferred

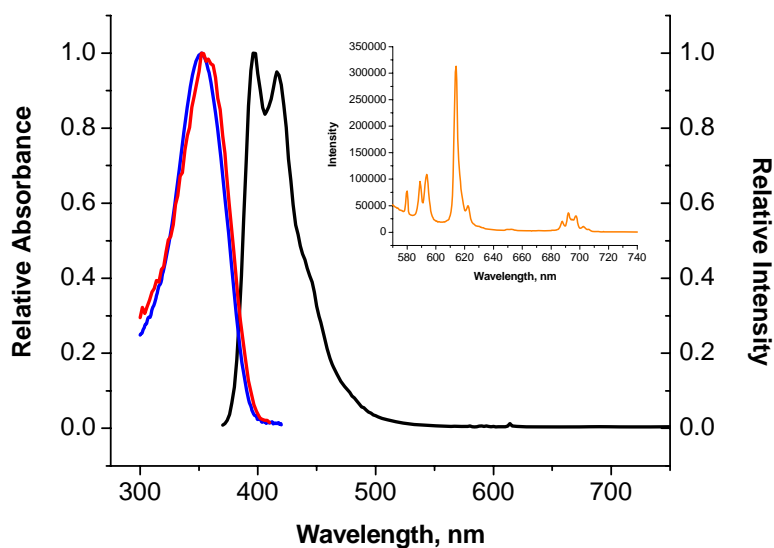efficiently from the terfluorene to the Tb^{3+} lanthanide cation.

Figure 27. Relative absorbance (blue), steady-state excitation (red: λ_{em} = 420 nm) and steady-state emission (black, λ_{ex} = 353 nm) of TF1:Tb^{3+} complex in CH_2Cl_2 (~10^{-6} M), 298 K.

The efficiency of terfluorene to lanthanide energy transfer as well as the quenching of the lanthanide metal ion, in both the TF1 Eu^{3+} and Tb^{3+} complexes, was quantitatively assessed through quantum yield measurements. These values were measured relative to the terbium 2-hydroxyisophthalamide complex in water (Φ = 0.59)[4]. The values are reported in **Table 3**. The high value of the TF1:Eu^{3+} complex quantum yield (CH_2Cl_2: 0.08 ± 0.002; DMSO: 0.07 ± 0.006) was due to small energy gap (~732 cm^{-1}) between the triplet state of the TF1 ligand and the lower energy accepting level of the europium cation ($^5D_0$, 17, 286 cm^{-1}). This quantum yield is about three times the value (QY ~ 2-3 %) of the Lehn europium cryptate complexes[39], used in fluoroimmunoassays, described in Chapter 4. The relatively low quantum yield of the TF1:Tb^{3+} complex (CH_2Cl_2: 0.007 ± 0.002; DMSO: 0.002 ± 0.001) was explained by the TF1 triplet state lying below the $^5D_4$ accepting level of Tb^{3+} in energy (~ 2, 527 cm^{-1}). This mismatch of donating and accepting energy levels suggested the presence of an energy back transfer from the Tb^{3+} to

the terfluorene moiety. Chapter 7 discusses the energy levels of the MF2 and TF1 ligands in

relation to the lanthanide excited states in more detail.

Table 3. Luminescence lifetimes centered on the lanthanide excited states and their respective quantum yields for the TF1 lanthanide complexes (~10-6 M), 298 K.

Sample Complex	Lifetimes (λ_{em}, transition) (ms)[b,d]	Quantum Yield[a,c,d]	Lifetimes (λ_{em}, transition) (ms)[b,e]	Quantum Yield[a,c,e]
TF1:Tb^{3+}	0.44 ± 0.05 0.160 ± 0.006 (545 nm, $^5D_4 \rightarrow {}^7F_5$)	0.007 ± 0.002	0.65 ± 0.16 0.11 ± 0.01 (545 nm, $^5D_4 \rightarrow {}^7F_5$)	0.002 ± 0.001
TF1:Eu^{3+}	1.60 ± 0.02 0.70 ± 0.07 (614 nm, $^5D_0 \rightarrow {}^7F_2$)	0.08 ± 0.002	1.46 ± 0.01 0.61 ± 0.01 (614 nm, $^5D_0 \rightarrow {}^7F_2$)	0.07 ± 0.006

a. Quantum yield measurements using TbH22IAM[4] in water as a reference (Φ = 0.59).
b. λ_{ex} = 354 nm.
c. λ_{ex} = 350 nm.
d. Measured in CH_2Cl_2.
e. Measured in DMSO.

The steady-state fluorene emission appeared as the most intense bands in these TF1

complexes. The two high energy singlet transitions (398 and 420 nm) and the one lower energy

shoulder (~ 440 nm) exhibited the characteristic shape of the fluorene emission[16]. The same

fluorene steady-state emission is depicted in **Figure 28** for the TF1:Gd^{3+} complex.

The steady-state emission spectra and quantum yields demonstrated that TF1 sensitized

Eu^{3+} and Tb^{3+}, with quenching energy back-transfer present in the terbium complex. Time-

resolved excitation spectra were used to assess the antenna effect, an important quality in

complexes where chromophores sensitize the lanthanide cation especially when the lanthanide

emission signal is not apparent in the steady-state mode (unlike the MF2 complexes in Chapter

5.2). The antenna's broad excitation band(s) are usually discriminated from the atom-like

excitation bands centered on the lanthanide cation. Thus, time-resolved excitation spectra, upon

monitoring Ln^{3+} emission, were excellent indicators for the antenna effect in the TF1 complexes.
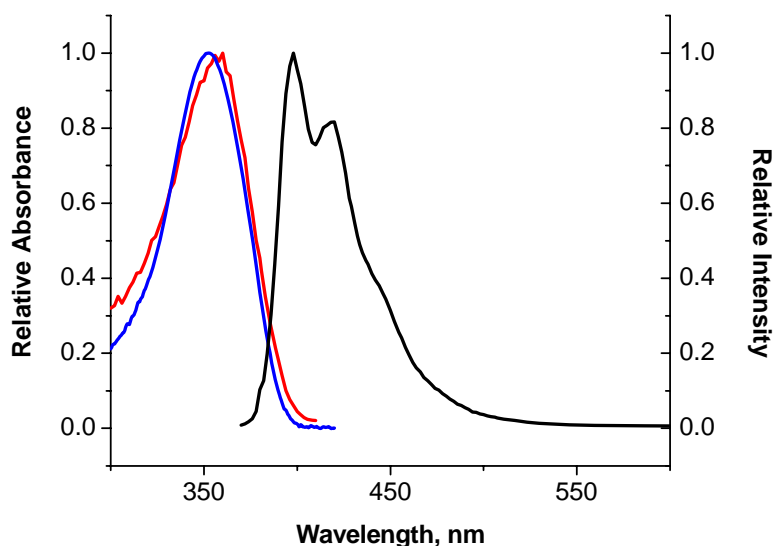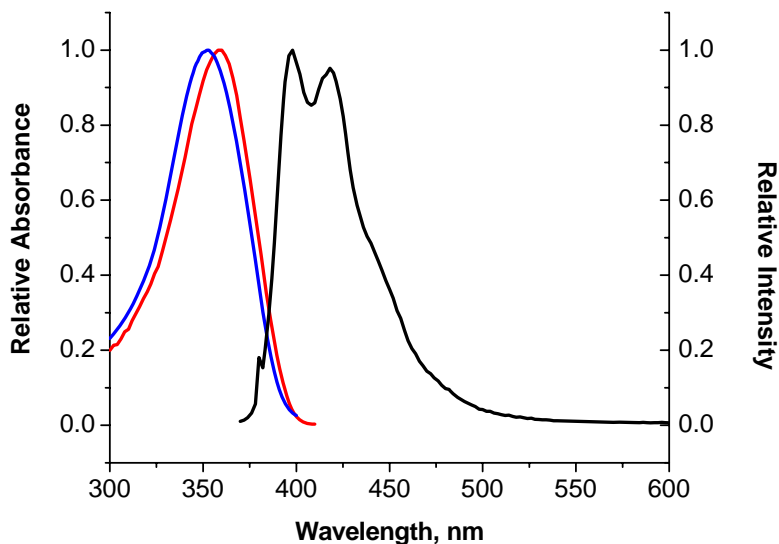

Figure 28. Relative absorbance (blue), steady-state excitation (red: λ_{em} = 420 nm) and steady-state emission (black, λ_{ex} = 353 nm) of TF1:Gd^{3+} complex in CH_2Cl_2 (~10^{-6} M), 298 K.

The time-resolved excitation spectra of the TF1:Eu^{3+} (**Figure 29**, red) and the TF1:Tb^{3+}

(**Figure 30**, green) complexes in CH_2Cl_2 both had a broad excitation band centered at 350 nm.

Time-resolved excitation spectra of $Eu(NO_3)_3$ (**Figure 29**, black) and $Tb(NO_3)_3$ (**Figure 30**,

black) are displayed as references of direct lanthanide excitation for the respective compounds.

The broad excitation bands in the time-resolved excitation spectra of the Eu^{3+} and Tb^{3+}

complexes did not resemble the sharp, direction excitation bands of the respective lanthanide

cations, which confirms the terfluorene served as an antenna, and that the lanthanide cations in

these complexes were not directly excited through lanthanide excited states.
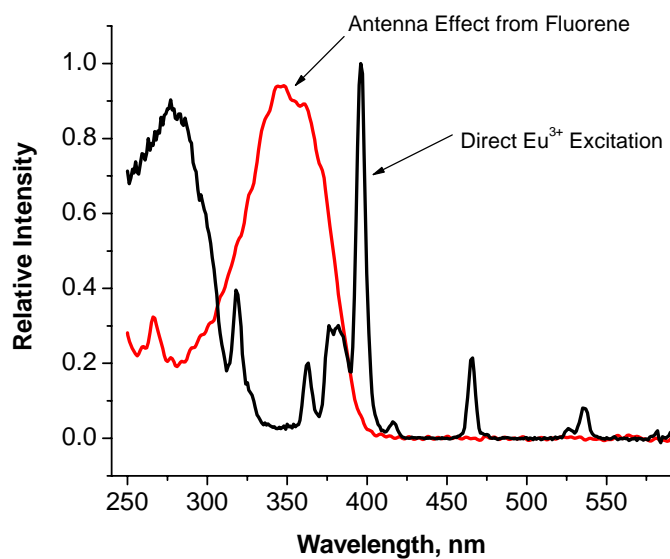
Figure 29. Time-resolved excitation spectra (normalized, 0.2 ms delay) of TF1:Eu^{3+} complex (red, ~10^{-6} M) and Eu(NO$_3$)$_3$ (black, 10 mM), both in CH$_2$Cl$_2$ (1% MeOH in CH$_2$Cl$_2$ for Eu(NO$_3$)$_3$ solution), 298 K. λ_{em} = 614 nm for both spectra.

The time-resolved emission spectrum of the TF1:Eu^{3+} complex (**Figure 31**) displayed similar, sharp emission bands at the same energy positions for both excitation wavelengths (267 and 347 nm). In the TF1:Tb^{3+} complex, the sharp, lanthanide emission bands of the two spectra also occurred at similar energy positions, despite excitation at different wavelengths (347 and 379 nm, **Figure 32**).
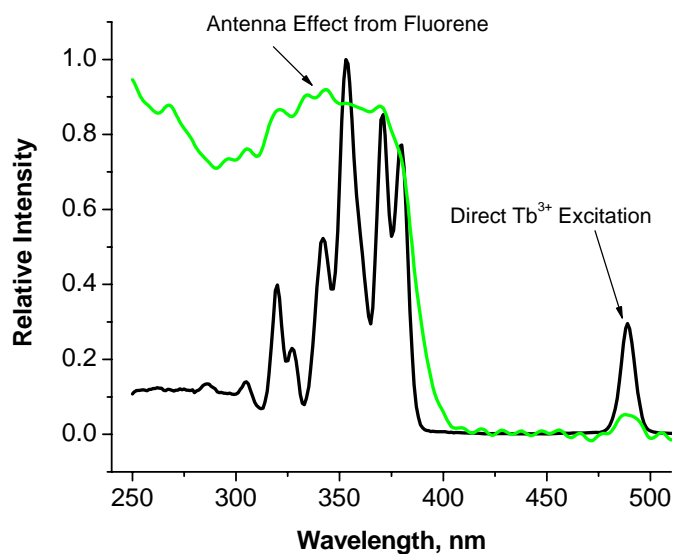
Figure 30. Time-resolved excitation spectra (normalized, 0.2 ms delay) of TF1:Tb^{3+} complex (green, ~10^{-6} M) and Tb(NO$_3$)$_3$ (black, 10 mM), both in CH$_2$Cl$_2$ (1% MeOH in CH$_2$Cl$_2$ for Tb(NO$_3$)$_3$ solution), 298 K. λ_{em} = 545 nm for both spectra.

Figure 31. Time-resolved emission spectra (normalized, 0.2 ms delay) of TF1:Eu^{3+} complex (~10^{-6} M) in CH$_2$Cl$_2$, 298 K (red: λ_{ex} = 347 nm, black: λ_{ex} = 267 nm, direct).
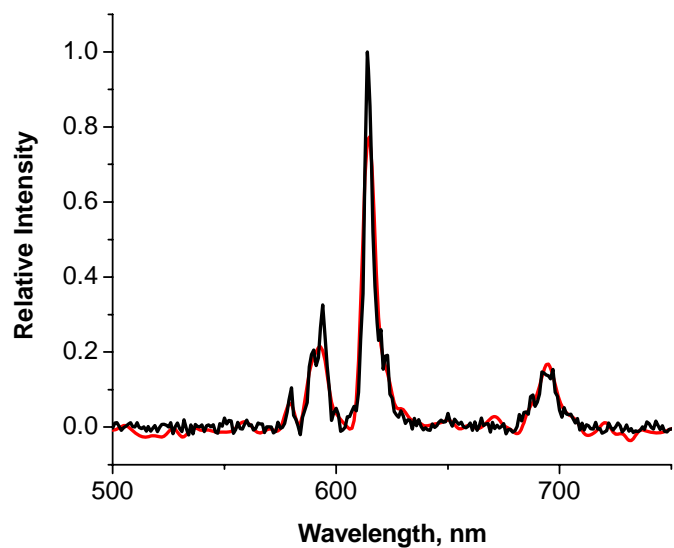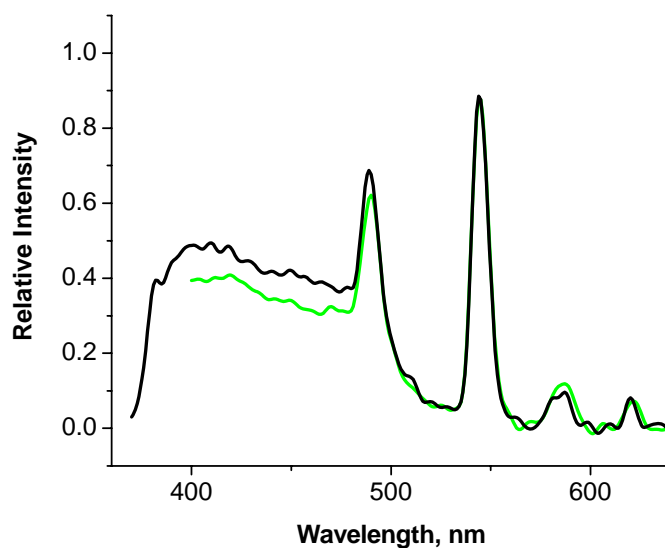
Figure 32. Time-resolved emission spectra (normalized, 0.2 ms delay) of TF1:Tb^{3+} complex (~10^{-6} M) in CH$_2$Cl$_2$, 298 K (red: λ_{ex} = 347 nm, black: λ_{ex} = 379 nm, direct).

6.3 LUMINESCENCE LIFETIME MEASUREMENTS (LANTHANIDE-CENTERED EMISSION, 298 K)

Luminescence lifetimes of the lanthanide emissive levels are displayed in **Table 3**. The lifetime values varied greatly between the two TF1 complexes. The experimental exponential decay of the TF1:Eu^{3+} complex fit best as a bi-exponential fitting, suggesting two different environments for the europium cation. The longer lifetime component in CH$_2$Cl$_2$, 1.60 ms, indicated a europium cation which was well protected from deactivation processes. The shorter lifetime, 0.70 ms, of the europium complex, also in CH$_2$Cl$_2$, was indicative of a cation less protected from non-radiative deactivation. This shorter component value was very similar to the lifetime value reported by Gulgas and Reineke[38]. They measured the lifetime of a europium cation (0.70 ms), also complexed in a DTPA moiety. They concluded the europium cation had one water molecule coordinated to its inner sphere. The TF1:Tb^{3+} complex had lifetime values much shorter than the

49

europium TF1 complex. This complex also had two different environments for the lanthanide

cation as well, given its bi-exponential fitting. The shortness of both lifetimes in each solvent

(0.44 and 0.160 ms in CH_2Cl_2, for example) was an indication of energy-back transfer in both

environments of the terbium cation. The terbium cation likely had the same degree of protection

as the europium cation in its respective complex; however, the severe mismatch of the accepting

level of the terbium cation and the terfluorene donating levels decreased both lifetime

components in the TF1:Tb^{3+}.

7.0   COMPARISON OF THE FLUORENE COMPLEX SYSTEMS

7.1   JABLONSKI DIAGRAMS AND TRIPLET STATES OF THE OLIGOFLUORENE COMPLEXES

The energies of the triplet states of the monofluorene and terfluorene complexes are key

components in assessing the efficiencies of energy transfer characteristics of the respective

complexes. Triplet states are central pathways for energy transfer between the ligand and

lanthanide cation. Measurement of the triplet state energies in the oligofluorene-lanthanide

complexes indicate whether changing the fluorene backbone length changes the discrete energy

of the chromophore. Complexes of gadolinium were prepared with the ligands MF2 and TF1,

both in DMSO. The triplet state energies of the complexes were measured in the presence of the

lanthanide cation Gd^{3+} because the accepting levels of Gd^{3+} (^6P_J) are high in energy. Moreover,

these accepting levels are sufficiently high (~32, 500 cm^{-1}) as not to quench the excited states on

the ligand.

Triplet states, centered on ligands in lanthanide complexes, are typically low in energy

and low in population. In addition, these low-lying states are more susceptible to quenching

through non-radiative deactivation. To increase the population of the triplet states and minimize

the probability of deactivation, the measurements are commonly performed with concentrated

samples (~ mM) and at low temperatures (77 K). The complexes of MF2:Gd^{3+} and TF1:Gd^{3+}

were prepared at 1 mM in DMSO. **Figure 33** depicts the time-resolved emission of the

51

respective complexes at 77 K (MF2:Gd^{3+}: λ_{ex} = 268 nm; TF1:Gd^{3+}: λ_{ex} = 353 nm). The

wavelengths corresponded to the excitation through the respective ligands in both spectra. Both

emission bands of the respective complexes were broad (~200 nm). The apparent maxima of the

band envelope for these emission bands for MF2:Gd^{3+} and TF1:Gd^{3+} were 442 and 555 nm,

respectively. Therefore, the apparent triplet state energies were 22624 cm^{-1} and 18018 cm^{-1} for

MF2:Gd^{3+} and TF1:Gd^{3+}, respectively.
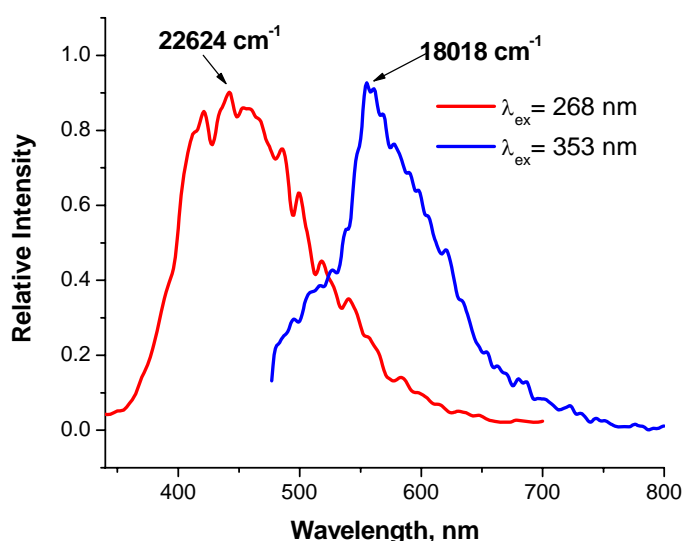
Figure 33. Time-resolved emission spectra of MF2:Gd^{3+} (red, λ_{ex} = 268 nm) and TF1:Gd^{3+} (blue, λ_{ex} = 353 nm) in DMSO, 1mM, 0.2 ms delay after flash. These spectra were collected at 77 K and the wavenumbers denote the energies of the apparent maxima of the band envelopes in the respective complexes.

Figure 34 displays the proposed Jablonski diagrams for the Eu^{3+} (top) and Tb^{3+} (bottom)

complexes of the MF2 ligand. The emission band centered on the monofluorene was expressed

as a singlet state at an energy position of 27, 855 cm^{-1} (359 nm). The energy gap between the

triplet state donating level and accepting levels of the respective lanthanides is also depicted for

each complex. 3, 598 cm^{-1} separated the triplet state donating level of the MF2 ligand (22, 624

cm^{-1}) from the $^5D_1$ accepting level of Eu^{3+} (19, 026 cm^{-1}). This relatively large energy gap

nevertheless corresponded to moderate quantum yield of about 1% through the europium. The energy gap between the triplet state and the $^5D_4$ (20, 545 cm^{-1}) accepting level of Tb^{3+} (2, 079 cm^{-1}) was smaller, however; and resulted in a more robust quantum yield through the lanthanide (~ 4.5%). The smaller gap in the MF2:Tb^{3+} complex resulted in more efficient (four-fold) energy transfer to the lanthanide cation than the MF2:Eu^{3+} complex.

Figure 34. Proposed Jablonski diagrams for the MF2:Eu^{3+} (top, green) and MF2:Tb^{3+} (bottom, red) complexes. The ground state energy of the monofluorene ligand was assigned to 0 cm^{-1}.

The energy of the triplet state donating level between the MF2 and TF1 ligands did indeed shift (~ 4, 600 cm^{-1}), probably due to extending the conjugation of the chromophore backbone. Lengthening the oligofluorene backbone discretely shifted the triplet state to lower energy. **Figure 35** presents the proposed Jablonski diagrams for the Eu^{3+} and Tb^{3+} TF1 complexes. The singlet state energy positions were calculated from the two maxima of terfluorene steady-state emission (400 nm: 25, 000 cm^{-1}; 420 nm: 23, 809 cm^{-1}). As the triplet state energy of the terfluorene decreased, so too did the energy gap between the triplet state

donating level of TF1 and the accepting levels of the respective lanthanide cations. The triplet state of terfluorene in the TF1:Eu^{3+} complex lies 732 cm^{-1} above the lowest accepting level of Eu^{3+} ($^5D_0$, 17, 286 cm^{-1}). The close match in energy between these levels resulted in an increased quantum yield (~ 7-8%) relative to the MF2:Eu^{3+}. The extension of the oligofluorene backbone in the TF1 ligand effectively tuned the ligand to the accepting level of Eu^{3+}, resulting in a more efficient energy transfer. The triplet state centered on TF1 was lower in energy relative to the lone accepting level of Tb^{3+}. Moreover, the $^5D_4$ level of Tb^{3+} was 2, 527 cm^{-1} higher in energy than the triplet state of TF1. This mismatch in energy between the two energy levels was reflective of the relatively low quantum yield (~ 0.2 - 0.7%) through Tb^{3+} in the TF1:Tb^{3+} complex. The low quantum yield was probably a result of energy back-transfer from the emitting level of terbium to the triplet state of TF1. The back-transfer due to the energy mismatch resulted in an overall poorly efficient system. The TF1:Eu^{3+} complex was more efficient than the TF1:Tb^{3+} complex by about 35-fold.

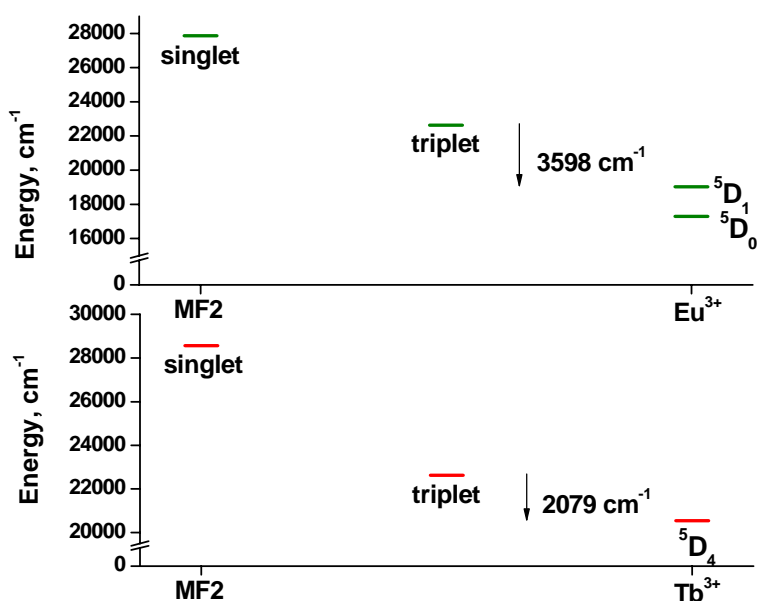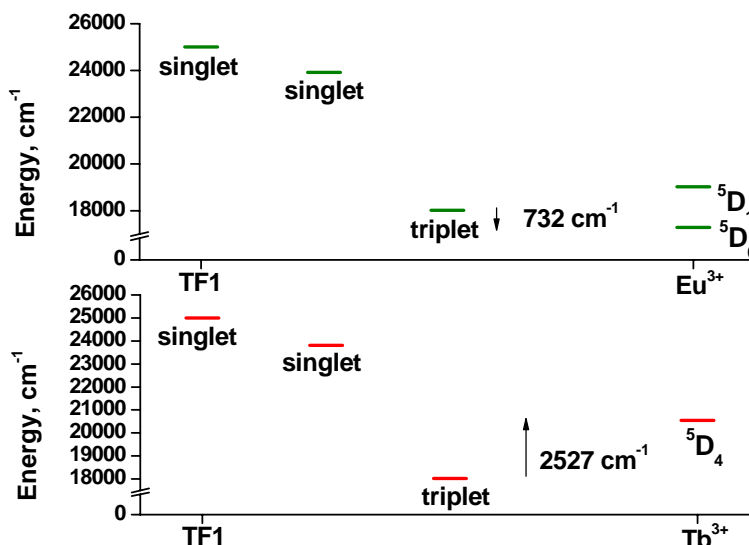**Figure 35. Proposed Jablonski diagrams for the TF1:Eu^{3+} (top, green) and TF1:Tb^{3+} (bottom, red) complexes. The ground state energy of the terfluorene ligand was assigned to 0 cm^{-1}.**

7.2 COMPARISON OF OLIGOFLUORENE LANTHANIDE COMPLEXES

The coordination of the lanthanide cations and isolation of the respective complexes was performed in the same manner with the three oligofluorene ligands. All luminescence lifetime values were expressed with bi-exponential decay fits, indicating that two different lanthanide cation environments existed in each respective complex. Each luminescent lanthanide cation had a long lifetime component (for a protected cation) and a short lifetime component (for a less protected cation). This result supported that the DTPA moiety was attached to the fluorene moiety in the same manner for each of the three ligands. The DTPA protected the lanthanide cations to the same degree in both the monofluorene (MF1 and MF2) and terfluorene (TF1) ligands.

The oligofluorene ligands induced different photophysical properties upon coordination to the luminescent lanthanide cations by providing different efficiencies of the antenna effect. For instance, a small structural change between the MF1 and MF2 ligands created a noticeable change in energy transfer. This was evidenced by the increase of lanthanide emission in the steady-state emission spectra of the MF2 complexes. This increase was attributed to removal of the butenyl wings, which removed a small amount of conjugation from the monofluorene chromophore backbone. The decrease in conjugation resulted in a 7 nm blue shift in the low energy absorption band of the monofluorene ligand (**Figure 36**). The small spectral shift allowed the fluorene electronic levels to access the lanthanide excited states more efficiently. Quantum yields of MF2:Tb^{3+} relative to MF1:Tb^{3+} supported the claim of increased efficiency.

The TF1:Eu^{3+} complex provided the most efficient system of energy transfer from the oligofluorene to the lanthanide cation (7-8% quantum yield), despite the absence of an intense europium signal in the steady-state emission spectrum. This discrepancy was explained by the large differences in molar absorptivities (ε, $M^{-1}cm^{-1}$) of the chromophores. **Figure 37** depicts the absorption spectra of the MF2:Gd^{3+} and TF1:Gd^{3+} complexes in DMSO. The ε value of the TF1 complex at its $\lambda_{abs, max}$ (352 nm, 21, 994 $M^{-1}cm^{-1}$) was approximately three times greater than the ε value of the MF2 at its $\lambda_{abs, max}$ (267 nm, 7, 409 $M^{-1}cm^{-1}$). The high ε value for the terfluorene moiety resulted in higher fluorescence intensity from the ligand, as shown in the steady-state emission spectra of the TF1 complexes. Relative to the monofluorene moiety, the terfluorene absorbed more light and emitted more light through its electronic levels, which skewed the apparent efficiency evidenced by the high quantum yield in the TF1:Eu^{3+} complex. The emission though the terfluorene moiety and the europium were concurrently favorable in the TF1:Eu^{3+} complex.
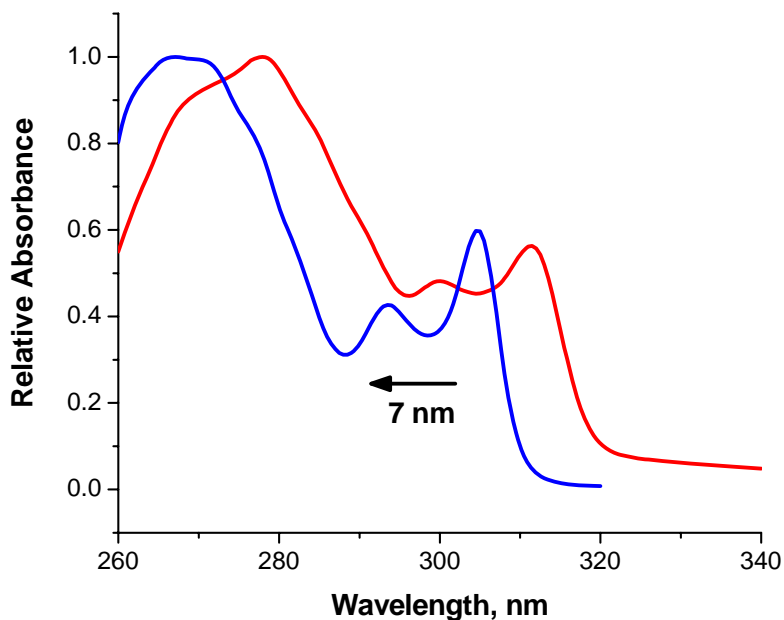

Figure 36. Relative absorbance spectra for the MF1:Gd^{3+} (red) and MF2:Gd^{3+} (blue) complexes. The spectra were collected at 298 K and at a concentration of 80 µM in DMSO.
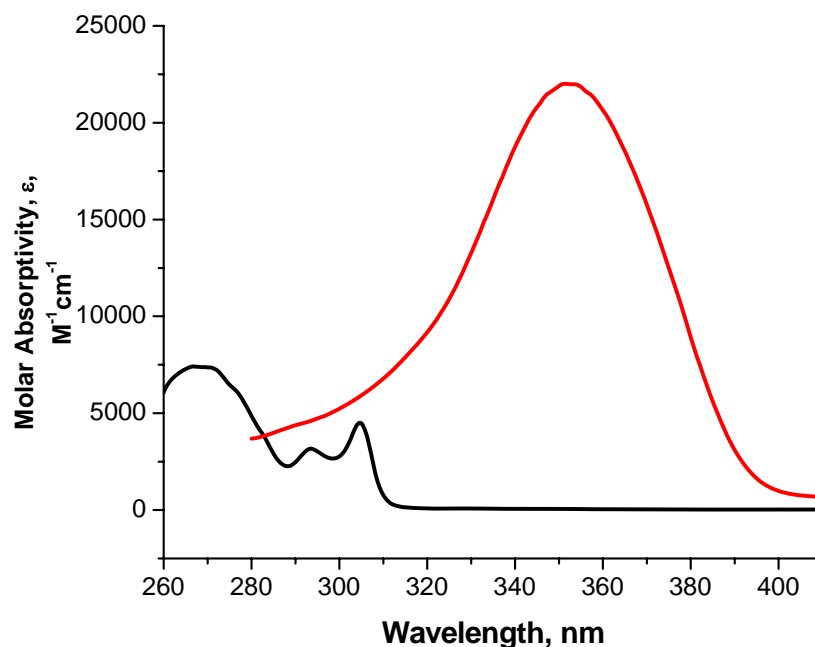
Figure 37. Absorption spectra for the MF2:Gd^{3+} (black) and TF1:Gd^{3+} (red) complexes. The spectra were collected at 298 K and at a concentration of 80 μM in DMSO.

The distinctive lanthanide complex in this set of systems was the TF1:Tb^{3+} complex. Several photophysical measurements collected on this complex indicated the presence of an efficient quenching through energy back-transfer between the Tb^{3+} excited state and the terfluorene moiety. The other five luminescent oligofluorene complexes demonstrated lanthanide emission in the steady-state mode and had at least one relatively long luminescence lifetime component (of the two components in the bi-exponential fit). These long luminescence lifetimes indicated that the different types of ligands well-protected a portion of the coordinated lanthanide cations.

7.3   CONCLUSIONS

The experimental results for these oligofluorene luminescent lanthanide complexes presented several conclusions. The three ligands (MF1, MF2 and TF1) functioned well as antennae, harvesting light and transferring the subsequent energy to the excited states of visibly emitting lanthanide cations. Protection of the lanthanide cations was sufficiently achieved by incorporating the DTPA moiety into the ligand for coordinating the cation, as evidenced by long lifetime components. Ligand to lanthanide energy transfer was demonstrated in the oligofluorene:Ln^{3+} complexes with values between 0.01 and 0.08 for lanthanide-centered quantum yields. These quantum yields rival the quantum yields of some commercially-available lanthanide compounds, with the TF1:Eu^{3+} demonstrating exceptional efficiency for a lanthanide complex. The ability to tune the electronic levels of several ligands to the accepting levels of luminescent lanthanide cations was demonstrated through a myriad of photophysical characterization.
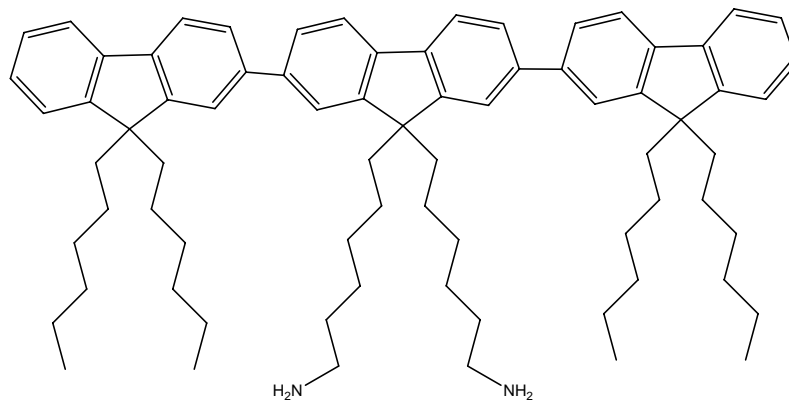
8.0   APPENDIX

Figure A1. Diamino terfluorene precursor, as received from Dr. James Copenhafer.

9.0 BIBLIOGRAPHY

1. Kaltsoyannis, N.; Scott, P., *The f Elements*. 1999: Oxford University Press.

2. Bünzli, J.-C.G.; Choppin, G.R., *Lanthanide Probes in Life, Chemical and Earth Sciences*. 1990: Elsevier Publishing.

3. Wong, K.-L.; Kwok, W.-M.; Wong, W.-T.; Phillips, D.L.; Cheah, K.-W., *Angewandte Chemie, International Edition* **2004**, 43(35), 4659-4662.

4. Petoud, S., Cohen, S.M.; Bünzli, J.-C.G.; Raymond, K.N., *Journal of the American Chemical Society* **2003**, 125(44), 13324-5.

5. Bünzli J.-C.G., *Acc. Chem. Res.* **2006**, 39(1), 53-61.

6. Weissman, S.I., *Journal of Chemical Physics* **1942**, 10, 214-7.

7. Dexter, D.L., *Journal of Chemical Physics* **1953**, 21, 836-50.

8. Forster, T., *Discussions of the Faraday Society* **1959**, 27, 7-17.

9. Faulkner, S.; Beeby, A.; Carrie, M.-C.; Dadabhoy, A.; Kenwright, A.M.; Sammes, P.G., *Inorganic Chemistry Communications* **2001**, 4(4), 187-190.

10. Turowski, P.N.; Rodgers, S.J.; Scarrow, R.C.; Raymond, K.N., *Inorganic Chemistry* **1988**, 27(3), 474-81.

11. Li, M.; P.R. Selvin, *Journal of the American Chemical Society* **1995**, 117(31), 8132-8.

12. Klaerner, G.; Miller, K.D., *Macromolecules* **1998**, 31(6), 2007-9.

13. Klaerner, G.; Lee, J.-I.; Davey, M.H.; Miller, R.D., *Advanced Materials* **1999**, 11(2), 115-9.

14. Wu, H.; Huang, F.; Mo, Y.; Yang, W.; Wang, D.; Peng, J.; Cao, Y., *Advanced Materials* **2004**, 16(20), 1826-1830.

15. Liu, B.; Gaylord, B.S.; Wang, S.; Bazan, G.C., *Journal of the American Chemical Society* **2003**, 125(22), 6705-14.

16. Neher, D., *Macromolecular Rapid Communications* **2001**, 22(17), 1365-1385.

17. Pei, Q.; Yang, Y., *Journal of the American Chemical Society* **1996**, 118(31), 7416-7417.

18. Delmond, S.; Letard, J.-F.; Lapouyade, R.; Rettig, W., *Journal of Photochemistry and Photobiology, A: Chemistry* **1997**, 105(2-3), 135-148.

19. Berggren, M.; Inganas, O.; Gustafsson, G.; Rasmusson, J.; Andersson, M.R.; Hjertberg, T.; Wennerstrom, O., *Nature* **1994**, 372, 444-6.

20. Teetsov, J.; Fox, M.A., *Journal of Materials Chemistry* **1999**, 9(9), 2117-2122.

21. Scurlock, R.D.; Wang, B.; Ogilby, P.R.; Sheats, J.R.; Clough, R.L., *Journal of the American Chemical Society* **1995**, 117(41), 10194-202.

22. Cheon, C.H.; Joo, S.-H.; Kim, K.; Jin, J.-I.; Shin, H.-W.; Kim, Y.-R., *Macromolecules* **2005**, 38(15), 6336-6345.

23. Buckley, A.R.; Rahn, M.D.; Hill, J.; Cabanillas-Gonzalez, J.; Fox, A.M.; Bradley, D.D.C., *Chemical Physics Letters* **2001**, 339(5,6), 331-336.

24. Burrows, H.D.; Seixas de Melo, J.; Serpa, C.; Arnaut, L.G.; Monkman, A.P.; Hamblett, I.; Navaratnam, S., *Journal of Chemical Physics* **2001**, 115(20), 9601-9606.

25. Burrows, H.D.; Arnaut, L.G.; Pina, J.; Seixas de Melo, J.; Chattopadhyay, N.; Alcacer, L.; Charas, A.; Morgado, J., *Chemical Physics Letters* **2005**, 402(1-3), 197-201.

26. Zhang, M.; Lu, P.; Ma, Y.; Shen, J., *Journal of Physical Chemistry B* **2003**, 107(27), 6535-6538.

27. Ego, C.; Marsitzky, D.; Becker, S.; Zhang, J.; Grimsdale, A.C.; Muellen, K.; MacKenzie, J.D.; Silva, C.; Friend, R.H., *Journal of the American Chemical Society* **2003**, 125(2), 437-443.

28. Tirapattur, S.; Belletete, M.; Drolet, N.; Leclerc, M.; Durocher, G., *Macromolecules* **2002**, 35(23), 8889-8895.

29. Shu, C.-F.; Dodda, R.; Wu, F.-I.; Liu, M.S.; Jen, A.K.Y., *Macromolecules* **2003**, 36(18), 6698-6703.

30. Gong, X.; Ostrowski, J.C.; Moses, D.; Bazan, G.C., *Advanced Functional Materials* **2003**, 13(6), 439-444.

31. O'Brien, D.F.; Giebeler, C.; Fletcher, R.B.; Cadby, A.J.; Palilis, L.C.; Lidzey, D.G.; Lane, P.A.; Bradley, D.D.C., *Synthetic Metals* **2001**, 116(1-3), 379-383.

32. Vyprachticky, D.; Cimrova, V.; Kukla, S.; Pavlackova, P., *Macromolecular Chemistry and Physics* **2006**, 207(3), 318-326.

33. Male, N.A.H.; Salata, O.V.; Christou, V., *Synthetic Metals* **2002**, 126(1), 7-10.

34. McGehee, M.D.; Bergstedt, T.; Zhang, C.; Saab, A.P.; O'Regan, M.B.; Bazan, G.C.; Srdanov, V.I.; Heeger, A.J., *Advanced Materials* **1999**, 11(16), 1349-1354.

35. Ling, Q.D.; Kang, E.T.; Neoh, K.G.; Huang, W., *Macromolecules* **2003**, 36(19), 6995-7003.

36. Prudencio, M.; Rohovec, J.; Peters, J.A.; Tocheva, E.; Boulanger, M.J.; Murphy, M.E.P.; Hupkes, H.-J.; Kosters, W.; Impagliazzo, A.; Ubbink, M., *Chemistry - A European Journal* **2004**, 10(13), 3252-3260.

37. Konings, M.S.; Dow, W.C.; Love, D.B.; Raymond, K.N.; Quay, S.C.; Rocklage, S.M., *Inorganic Chemistry* **1990**, 29(8), 1488-91.

38. Gulgas, C.G.R.; Reineke, T.M., *Inorganic Chemistry* **2005**, 44(26), 9829-9836.

39. Mathis, G., *Clinical Chemistry* **1993**, 39(9), 1953-9.

40. Selvin, P.R.; Jancarik, J.; Li, M.; Hung, L.-W., *Inorganic Chemistry* **1996**, 35(3), 700-5.

41. Smith, J.A.; Brzezinska, K.R.; Valenti, D.J.; Wagener, K.B., *Macromolecules* **2000**, 33(10), 3781-3794.